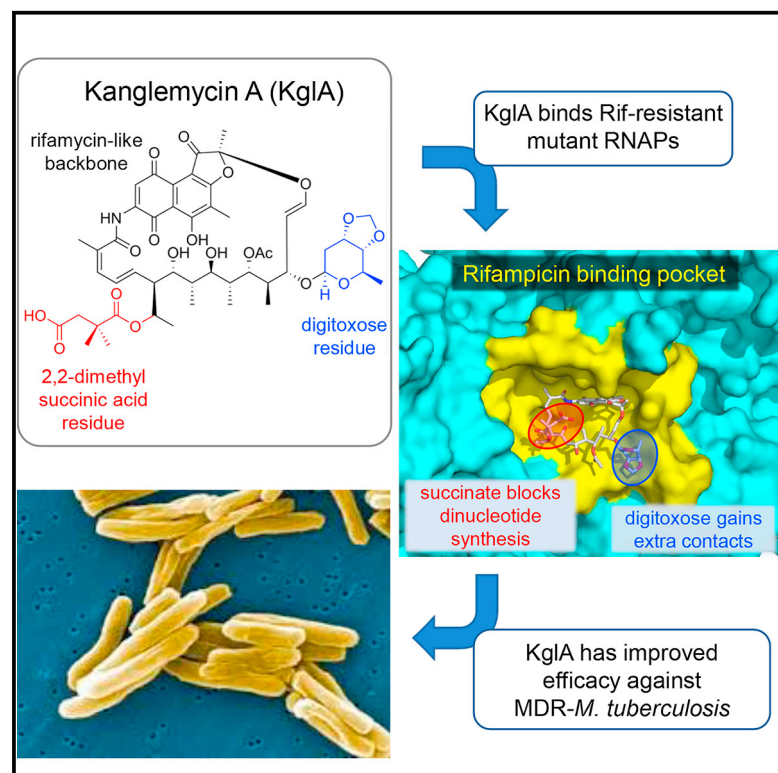# Mode of Action of Kanglemycin A, an Ansamycin Natural Product that Is Active against Rifampicin-Resistant *Mycobacterium tuberculosis*

Graphical Abstract

Authors

Hamed Mosaei, Vadim Molodtsov, Bernhard Kepplinger, ..., Michael John Hall, Katsuhiko S. Murakami, Nikolay Zenkin

Correspondence

kum14@psu.edu (K.S.M.), n.zenkin@ncl.ac.uk (N.Z.)

In Brief

Resistance to rifamycins, inhibitors of bacterial RNA polymerase used for treatment of tuberculosis, is increasing. Mosaei et al. report an analog of the rifamycins, kanglemycin A, that inhibits rifampicin-resistant RNA polymerases and is effective against multidrug-resistant *M. tuberculosis*, and they describe its mechanism of action.

Highlights

- Rifamycin kanglemycin A (KglA) inhibits rifampicin-resistant RNA polymerases (RNAPs)

- KglA's extra groups improve binding to RNAP and block first dinucleotide formation

- KglA is effective against multidrug-resistant *M. tuberculosis*

CellPress

Cell^{Press}

Mode of Action of Kanglemycin A, an Ansamycin Natural Product that Is Active against Rifampicin-Resistant *Mycobacterium tuberculosis*

Hamed Mosaei,[1,7] Vadim Molodtsov,[2,7] Bernhard Kepplinger,[1,3,7] John Harbottle,[1] Christopher William Moon,[4] Rose Elizabeth Jeeves,[4] Lucia Ceccaroni,[1] Yeonoh Shin,[2] Stephanie Morton-Laing,[5] Emma Claire Louise Marrs,[6] Corinne Wills,[5] William Clegg,[5] Yulia Yuzenkova,[1] John David Perry,[6] Joanna Bacon,[4] Jeff Errington,[1,3] Nicholas Edward Ellis Allenby,[3] Michael John Hall,[5] Katsuhiko S. Murakami,[2,*] and Nikolay Zenkin[1,8,*]

[1]Centre for Bacterial Cell Biology, Institute for Cell and Molecular Biosciences, Newcastle University, Newcastle upon Tyne NE2 4AX, UK
[2]Department of Biochemistry and Molecular Biology, The Center for RNA Molecular Biology, Pennsylvania State University, University Park, PA 16802, USA
[3]Demuris Limited, Newcastle Biomedicine Bio-Incubators, Framlington Place, Newcastle upon Tyne NE2 4HH, UK
[4]TB Research Group, National Infection Service, Public Health England, Manor Farm Road, Porton, Salisbury SP4 0JG, UK
[5]Chemistry, School of Natural and Environmental Sciences, Newcastle University, Newcastle upon Tyne NE1 7RU, UK
[6]Microbiology Department, Freeman Hospital, Newcastle upon Tyne NE7 7DN, UK
[7]These authors contributed equally
[8]Lead Contact
*Correspondence: kum14@psu.edu (K.S.M.), n.zenkin@ncl.ac.uk (N.Z.)
https://doi.org/10.1016/j.molcel.2018.08.028

SUMMARY

Antibiotic-resistant bacterial pathogens pose an urgent healthcare threat, prompting a demand for new medicines. We report the mode of action of the natural ansamycin antibiotic kanglemycin A (KglA). KglA binds bacterial RNA polymerase at the rifampicin-binding pocket but maintains potency against RNA polymerases containing rifampicin-resistant mutations. KglA has antibiotic activity against rifampicin-resistant Gram-positive bacteria and multidrug-resistant *Mycobacterium tuberculosis* (MDR-*M. tuberculosis*). The X-ray crystal structures of KglA with the *Escherichia coli* RNA polymerase holoenzyme and *Thermus thermophilus* RNA polymerase-promoter complex reveal an altered—compared with rifampicin—conformation of KglA within the rifampicin-binding pocket. Unique deoxysugar and succinate *ansa* bridge substituents make additional contacts with a separate, hydrophobic pocket of RNA polymerase and preclude the formation of initial dinucleotides, respectively. Previous *ansa*-chain modifications in the rifamycin series have proven unsuccessful. Thus, KglA represents a key starting point for the development of a new class of *ansa*-chain derivatized ansamycins to tackle rifampicin resistance.
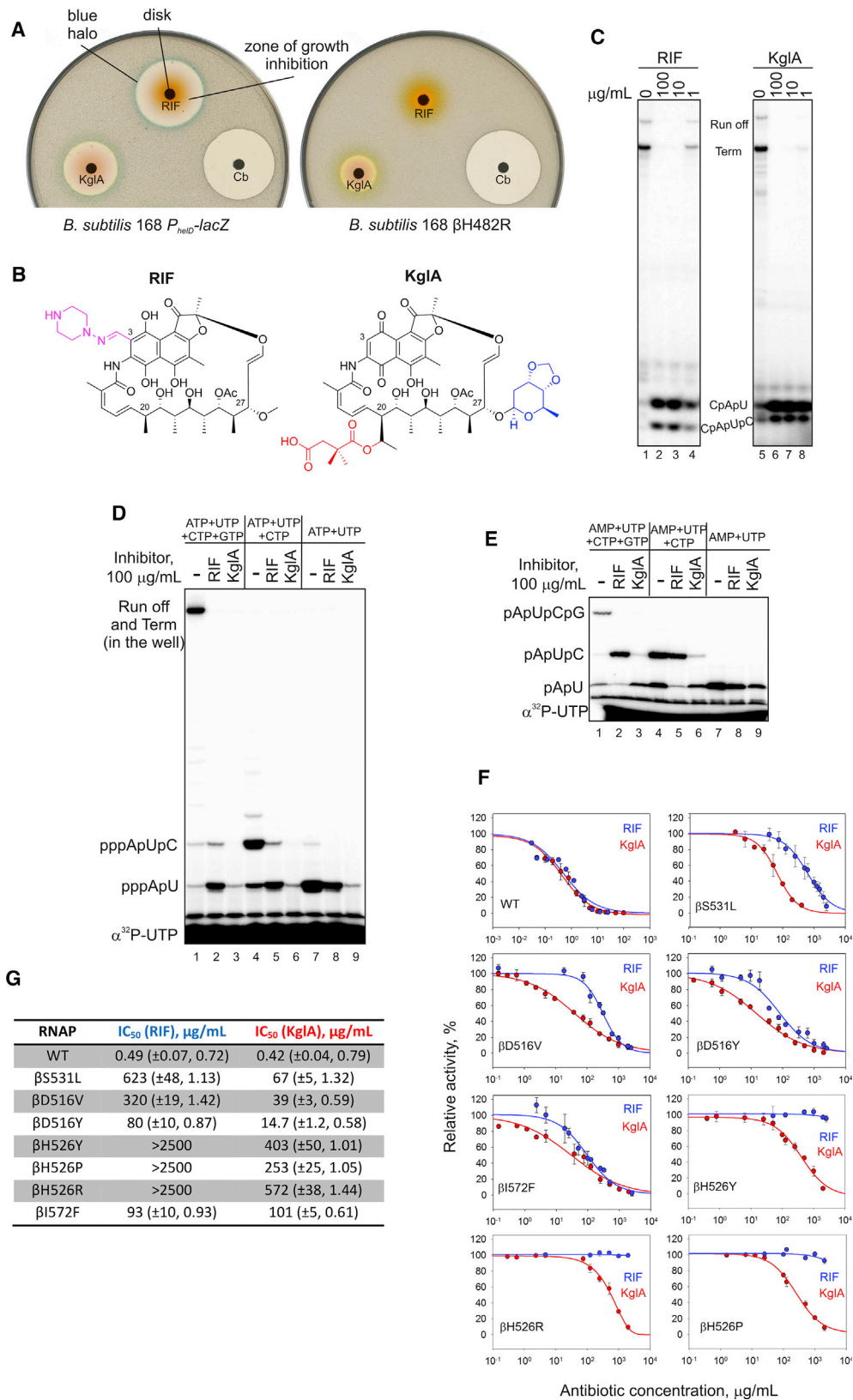
INTRODUCTION

Antibiotic resistance is on the increase, exacerbated by the fact that, in recent years, only a few new compounds have reached

the clinic. RNA polymerase (RNAP) is an essential enzyme accomplishing transcription in all living organisms. At the same time, the sequence divergence between bacterial and human RNAPs makes bacterial RNAP an excellent target for antibiotic development (Ho et al., 2009). In the last few years, details of the mode of action of a number of inhibitors of RNAP have been described (Bae et al., 2015; Degen et al., 2014; Maffioli et al., 2017; Molodtsov et al., 2015; Mukhopadhyay et al., 2008; Zhang et al., 2014a). However, most of these molecules have limited clinical utility, mainly because of their poor penetration of the bacterial cell envelope or strong binding to human plasma protein. Nevertheless, the search for new molecules that target RNAP and analysis of their mode of action is a promising approach for the development of new antibiotics, as exemplified by the now clinically used fidaxomicin (trade name Dificid) for *Clostridium difficile*-associated diarrhea (Tupin et al., 2010).

The most studied class of antibiotics known to inhibit bacterial RNA transcription are the rifamycins, a family of mainly semisynthetic ansamycins derived from the natural product rifamycin S, of which rifampicin (RIF) is the most widely used (Aristoff et al., 2010). RIF (and the other rifamycins) binds in a pocket (the RIF pocket) on the β subunit of RNAP in the vicinity of the catalytic site and sterically blocks propagation of the growing RNA chain through the main channel of RNAP (Campbell et al., 2001; McClure and Cech, 1978). The collision of RNA and RIF happens when the RNA reaches a length of 3–4 nucleotides, after which the RNA is released from the promoter complex as an abortive transcript. The length of the abortive RNA product can be influenced by the nature of the C3 substituent of the individual semisynthetic rifamycin. For example, rifabutin even inhibits synthesis of a trinucleotide (when reaction is started with a 5′-nonphosphorylated dinucleotide primer), whereas RIF still allows it (Artsimovitch et al., 2005).

The rifamycins are used, as part of the current combination therapy, for the first-line treatment of tuberculosis (TB), the

A

blue halo   disk   zone of growth inhibition

B. subtilis 168 P*helD*-*lacZ*   *B. subtilis* 168 βH482R

B

RIF   KglA

C

RIF   KglA

μg/mL

Run off
Term

CpApU
CpApUpC

1 2 3 4   5 6 7 8

D

Inhibitor, 100 μg/mL

	ATP+UTP +CTP+GTP			ATP+UTP +CTP			ATP+UTP		
	-	RIF	KglA	-	RIF	KglA	-	RIF	KglA

Run off
and Term
(in the well)

pppApUpC

pppApU

α³²P-UTP

1 2 3 4 5 6 7 8 9

E

Inhibitor, 100 μg/mL

	AMP+UTP +CTP+GTP			AMP+UTP +CTP			AMP+UTP		
	-	RIF	KglA	-	RIF	KglA	-	RIF	KglA

pApUpCpG

pApUpC

pApU

α³²P-UTP

1 2 3 4 5 6 7 8 9

F

Relative activity, %

WT   βS531L   βD516V   βD516Y   βI572F   βH526Y   βH526R   βH526P

RIF   KglA

Antibiotic concentration, μg/mL

G

RNAP	IC$_{50}$ (RIF), μg/mL	IC$_{50}$ (KglA), μg/mL
WT	0.49 (±0.07, 0.72)	0.42 (±0.04, 0.79)
βS531L	623 (±48, 1.13)	67 (±5, 1.32)
βD516V	320 (±19, 1.42)	39 (±3, 0.59)
βD516Y	80 (±10, 0.87)	14.7 (±1.2, 0.58)
βH526Y	>2500	403 (±50, 1.01)
βH526P	>2500	253 (±25, 1.05)
βH526R	>2500	572 (±38, 1.44)
βI572F	93 (±10, 0.93)	101 (±5, 0.61)

(legend on next page)

leading cause of death by infectious disease worldwide (World Health Organization, 2017), as well as treatment for non-tuberculous mycobacterial infections (Ryu et al., 2016). One of the major problems with known rifamycins is the rapid selection for mutations in the RIF-binding pocket of RNAP that lead to resistance. Multidrug-resistant strains of *Mycobacterium tuberculosis* (MDR-*M. tuberculosis*) present a major clinical problem because these strains are resistant to RIF in addition to isoniazid. In 2016, there were 600,000 new cases with resistance to RIF, of which 490,000 had MDR-TB. With a treatment success rate of only 54%, this highlights the requirement for improved treatment options. There are ~100 different amino acid substitutions in the RIF pocket that have been found in RIF-resistant clinical isolates of *M. tuberculosis* (Sandgren et al., 2009), with mutations at three positions of the RIF pocket that account for ~70% of the total substitutions (D516, 7.4%; H526, 20%; S531, 42%; *E. coli* numbering).

Previous efforts to probe the structure-activity relationships of the rifamycins and, thus, to maximize their binding affinity for RNAP have shown that the minimum structural requirements essential for activity include two free hydroxyl groups at the C21 and C23 positions of the *ansa* chain and two polar (free hydroxyl or carbonyl) groups at the C1 and C8 positions of the napthoquinone ring. Furthermore the molecule must be able to adopt a specific conformational geometry to position these key functional groups in the correct spatial arrangement required for RNAP binding (Bacchi et al., 1998; Lancini and Zanichelli, 1977). Thus, modification of the *ansa* bridge (e.g., hydrogenation or epoxidation of the C16,17 or C18,19 carbon-carbon double bonds) results in decreased binding to RNAP because of conformational changes in the molecule altering the spatial arrangement of the C1, C8, C21, and C23 functional groups, thus disrupting their critical hydrogen bonds with the RIF pocket (Aristoff et al., 2010; Bacchi et al., 2008). Hence, the production of clinically used semisynthetic rifamycins (RIF, rifabutin, rifapentine, rifalazil, and rifaximin) has focused on the introduction of functionality at the C3 position to stabilize the oxidation state of the naphthoquinone core and to improve bioavailability (Floss and Yu, 2005; Perlman, 1977).

Here we isolated and, by using microbiological, biochemical, and structural biology techniques, studied an uncharacterized naturally produced antibiotic, kanglemycin A (KglA). KglA is an ansamycin antibiotic from the rifamycin family that displays two important and unusual *ansa* bridge modifications. We show that, despite having a mode of action similar to that of

RIF, KglA has a larger binding surface with the RNAP provided by interactions of the *ansa*-bridge substituents and areas of RNAP that have not been previously accessible by rifamycin derivatives. As a result, KglA has an altered binding conformation compared with RIF, which makes it maintain higher activity against both RIF-resistant RNAPs and RIF-resistant bacteria.

RESULTS

Isolation of KglA

Actinomycete bacteria have historically been an excellent source of bioactive compounds, particularly antibiotics. To identify new antibiotics targeting transcription, we screened a subset of strains from the Demuris collection of actinomycetes for their ability to inhibit cell growth and to inhibit cellular transcription. As a reporter strain, we used a previously described *B. subtilis* strain that has a *lacZ* gene fused to the promoter of the bacterial helicase *helD*. This promoter was selected as the one that is up-regulated during the stress caused by partial inhibition of transcription in sub-inhibitory concentrations of an antibiotic (Urban et al., 2007a). In the disk assay shown in Figure 1A, when a paper disk soaked with antibiotic is placed on the X-gal-infused agar plate with a lawn of growing cells, this results in a colorimetric response at the edge of the zone of growth inhibition, observed as a blue halo (Figure 1A, left; compare the halos produced by RIF and carbenicillin, an inhibitor of cell wall synthesis). The isolate *Amycolatopsis* DEM30355 was of particular interest because it produced a compound (later identified as KglA, see below) that gave a blue halo at the edge of the zone of bacterial growth inhibition, indicative of transcription inhibition (Figure 1A, left). Importantly, in contrast to RIF, this new compound inhibited the RIF-resistant *B. subtilis* strain (βH482R; βH526R in *E. coli* numbering) (Figure 1A, right). We cultivated *Amycolatopsis* DEM30355 in a stirred tank bioreactor for 103.5 hr and extracted the secondary metabolites from the supernatant using Amberlite XAD-16 beads. Subsequent elution with methanol, extraction with ethyl acetate, and purification by multistep chromatography (STAR Methods) produced an orange crystalline compound that retained the observed biological activity against both the reporter and RIF-resistant strains (Figure 1A). Electrospray ionization-mass spectrometry (ESI-MS) revealed the mass, $[M+Na]^+ = 1004.3866$ m/z (Figure S1A), which corresponded to the mass of the previously described KglA. ^{1}H and ^{13}C nuclear magnetic resonance (NMR), extensive 2D NMR analysis, and, finally, single-crystal X-ray analysis (Figures S1B–S1D;

Figure 1. Identification and Mode of Action of KglA

(A) Disk diffusion assay with rifampicin (RIF), carbenicillin (Cb), and kanglemycin A (KglA). Paper disks soaked with antibiotics were placed on the lawns of wild-type *B. subtilis* carrying the *lacZ* gene under the P_{helD} promoter, inducible during partial inhibition of transcription (left), and RIF-resistant *B. subtilis* (right). Note the blue halo around the growth inhibition zones in the case of transcription inhibitors.

(B) Chemical structure of KglA in comparison with RIF. The *ansa* chain modifications in KglA are highlighted. The semisynthetic group of RIF is shown in purple. See also Figure S1 and Table S1.

(C) Transcription *in vitro* by *E. coli* RNAP started with CpA on a linear template containing the T7A1 promoter. Runoff, termination, and abortive tri- and tetra-nucleotides are marked. Note that tetra-nucleotides migrate faster than tri-nucleotides under these electrophoretic conditions.

(D) Different ratio of the di-nucleotide-long (pppApU) and the tri-nucleotide-long (pppApUpC) abortive products in the presence of RIF and KglA. Transcription was performed in the presence of the nucleotides depicted (in the absence of the CpA primer). Note that, in the 33% gel, runoff and termination products remain in the well.

(E) The experiment was performed as in (D) but in the presence of AMP instead of ATP.

(F and G) Inhibition of wild-type and RIF-resistant *E. coli* RNAPs by RIF and KglA. Error bars (F) are ± SD. The brackets (G) contain ± SE and the Hill slope.

Table S1) unambiguously confirmed the structure of the isolated compound to be KglA (Figure 1B).

KglA is an antibiotic originally isolated from the fermentation broth of *Nocardia mediterranei* var. *kanglensis* 1741-64 (Wang et al., 1988), for which no mode of action has been previously proposed, and only limited information regarding its biological activity has been reported. It is an ansamycin antibiotic that shares similarities with rifamycins, albeit with a number of unusual structural features. Most notably, KglA differs from known rifamycins and their semisynthetic derivatives in that it contains two large *ansa* bridge substituents, a pendant 2,2-dimethyl succinic acid side chain at C20 and a unique sugar moiety (β-*O*-3,4-*O,O'*-methylene digitoxose) at C27 (Figure 1B). Furthermore, these modifications are unusual for bioactive natural and semisynthetic rifamycins, whose modifications are typically concentrated at the naphthoquinone core.

Mode of Action and Specificity of KglA

Activation of the *helD* promoter and its structural similarity to the rifamycins suggested that KglA targets bacterial RNAP. Therefore, we analyzed the effects of KglA on *in vitro* transcription by wild-type *E. coli* RNAP. KglA efficiently inhibited transcription on a linear DNA template containing the strong T7A1 promoter (Figure 1C). Inhibition of full-sized RNA products (run off or terminated) coincided with increased accumulation of short abortive tri- and tetra-nucleotide products (Figure 1C; the reactions were started with the dinucleotide primer CpA). Such a mode of action is characteristic of the rifamycins (Campbell et al., 2005; McClure and Cech, 1978), as can be seen from the pattern of inhibition of transcription by RIF (Figure 1C). In this mode of action, the antibiotic binds in the pathway of the nascent RNA, physically blocking its extension and inducing the release of short RNAs as abortive products.

Dinucleotide primer CpA that was used to start transcription does not carry a negatively charged triphosphate moiety at the 5′ end, which is present in NTPs used by RNAP *in vivo*. Therefore, we analyzed the effects of RIF and KglA in a native situation when transcription was started with ATP (in the absence of the CpA primer). As can be seen in Figure 1D, KglA completely blocked the formation of the triphosphorylated trinucleotide, pppApUpC, whereas RIF allowed some of its production (compare lanes 4, 5, and 6). Furthermore, KglA strongly diminished (70-fold inhibition) the formation of the first dinucleotide, pppApU, whereas RIF had only a moderate effect (3-fold inhibition) (compare lanes 7, 8, and 9). Next, to start the reaction, we used AMP, which lacks γ and β 5′ phosphates, present in ATP (Figure 1E). KglA only moderately inhibited formation of pApU (4-fold), suggesting that it is γ and, possibly, β phosphates at the 5′ end of the initiating nucleotide that clash with the additional groups of KglA (compare lanes 7, 8, and 9). However, the formation of trinucleotide pApUpC was still strongly inhibited by KglA compared with RIF (Figure 1E, lanes 4, 5, and 6). These results further suggest that extra groups and/or the mode of binding of KglA provide an additional steric and/or electrostatic (KglA has a negatively charged C20 2,2-dimethyl succinic acid side chain) hindrance for translocation of the 5′ phosphorylated dinucleotide RNA. Furthermore, KglA interference with the 5′ triphosphate moiety of the initiating

nucleotide leads to inhibition even of the first phosphodiester bond formation (see structural support for these findings below).

The half maximal inhibitory concentration (IC_{50}) values of KglA and RIF were similar against wild-type RNAP (Figures 1G and 1F). However, despite having a similar mode of action as RIF, we observed that KglA killed RIF-resistant bacteria (compare the inhibition zones in Figure 1A, right). To investigate this phenomenon, we prepared *E. coli* RNAPs carrying a series of RIF-resistant mutations, including βS531L, βD516V, βD516Y, βH526Y, βH526P, βH526R, and βI572F. These mutations correspond to the RIF resistance mutations in *M. tuberculosis* most frequently observed in clinical isolates, with βS531L, βD516V, and βH526Y accounting for 73% of all clinical RIF-resistant *M. tuberculosis* isolates (Gill and Garcia, 2011). Compared with RIF, KglA was much more potent against six of seven RIF-resistant RNAPs (Figures 1G and 1F); in particular, KglA was 10 times more active than RIF against the βS531L and βD516V mutants. Note that, although mutations at βH526 made RNAP insensitive to RIF (no inhibition at 2.5 mg/mL), KglA was still able to inhibit RNAPs with these mutations.

These results and *in vivo* data (Figure 1A) suggest that KglA binds to RNAP in the RIF-binding pocket of the β subunit but in a manner different from known rifamycins, resulting in an increased resilience to the RIF-resistant amino acid substitutions in the RIF-binding pocket of RNAP. Furthermore, the mode of action of KglA deviates from that of RIF because KglA more efficiently inhibits the early stages of RNA synthesis.

Structural Basis of RNAP Inhibition by KglA

To reveal the basis of the KglA efficacy enhancement as induced by the modifications of the *ansa* bridge in comparison with rifamycin, we performed a crystallographic analysis of the complexes of KglA with RNAPs. To analyze the RNAP and KglA interaction on the atomic scale, a crystal of the *T. thermophilus* RNAP σ^A holoenzyme-*pyrG* promoter DNA complex (Murakami et al., 2017) was used to determine the X-ray crystal structure of the RNAP-KglA complex at 3.0-Å resolution (Table 1). Additionally, to understand the mechanism of inhibition of RIF-resistant RNAP by KglA, the crystal of the *E. coli* βS531L RNAP σ^{70} holoenzyme (Molodtsov et al., 2017) was used to determine the structure of the RNAP-KglA complex at 4.1-Å resolution (Table 1). The electron density maps of both RNAPs show unambiguous densities for the compound located in the RIF-binding pockets in the β subunits (Figures 2A and 2B). The binding modes of KglA to the RNAPs are almost identical; therefore, the atomic resolution structure of *T. thermophilus* RNAP-KglA was used for the precise modeling of KglA in complex with *E. coli* RNAP.

The binding mode of KglA is similar to that of RIF and involves the formation of hydrogen bonds with the same amino acid residues of the RIF-binding pocket, including βQ393, βS411, and βR420 (side chain) and βF394 (main chain) (Figures 2C and S2A; the numbering is for *T. thermophilus*; see Figures S2C and S2D for the corresponding amino acid residues in *E. coli* and *M. tuberculosis* RNAPs). Because of a different topology of the *ansa* bridge of KglA (Figure S2B), the C23 hydroxyl group does not form an additional hydrogen bond with βF394, as observed in the *T. thermophilus* RNAP-RIF complex. However,

Table 1. Collection of Crystallographic Data and Refinement Statistics

Complex	*Eco* RNAP – KglA	*Tth* RNAP – KglA
PDB code	6CUX	6CUU
Data Collection		
Space group	$P2_12_12_1$	C2
Cell dimensions		
a (Å)	188.167	185.221
b (Å)	204.685	101.315
c (Å)	311.577	294.279
β (°)	90	98.886
Resolution (Å)	50.0–4.1	50.0–3.0
Total reflections	608,898	358,319
Unique reflections	93,684	107,473
Redundancy	6.5 (6.2)	3.3 (3.0)
Completeness (%)[a]	99.9 (100.0)	99.7 (97.1)
I / σ[a]	16.2 (1.95)	10.2 (1.14)
R_{sym} (%)[a]	7.7 (85.1)	9.6 (61.4)
$CC^{1/2}$[a]	(0.633)	(0.629)
Refinement		
Resolution (Å)	45.03–4.1	46.3–3.0
R_{work}	0.2100	0.2012
R_{free}	0.2547	0.2483
No. of atoms	54,867	28,254
RMSDs		
Bond length (Å)	0.013	0.006
Bond angles (°)	1.776	1.089
Clashscore	11.47	5.84
Ramachandran favored, %	91.57	97.64
Ramachandran outliers, %	0.94	0.35

RMSD, root-mean-square deviation.
[a]Highest-resolution shells are shown in parentheses.

the C27 β-*O*-3,4-*O,O'*-methylene digitoxose side chain establishes a hydrogen bond with the side chain of βR134 (Figure 2C). This KglA *ansa* bridge side chain inserts into a shallow pocket in the RIF-binding site and establishes additional non-polar interactions with the surrounding residues, significantly increasing the binding surface of KglA compared with RIF (Figure 2C). One of the structural consequences of the sugar side chain accommodation in the RIF-binding pocket is a rotational shift of KglA that increases the distance between the naphthalene core and the binding surface of the pocket compared with RIF (Figure 2D).

To validate the new interaction of the C27 β-*O*-3,4-*O,O'*-methylene digitoxose side chain with βR134, we constructed an *E. coli* RNAP carrying a mutation at the corresponding amino acid residue, βR143A. The mutation had little effect on RIF sensitivity (Figure S2E, left). However, KglA was at least an order of magnitude less effective against βR143A RNAP than against wild-type RNAP, indicating the importance of this interaction

for KglA binding (Figure S2E, center). The IC_{50} of KglA for βR143A RNAP was still lower than for any RIF-resistant mutant RNAP, indicating that interactions of KglA within the rest of the RIF-binding pocket were still critical for its binding. Only a double mutation, βR143A/S531L, led to KglA resistance (Figure S2E, right).

The presence of additional bulky side chains on the *ansa* bridge of KglA has an effect on the mechanism of *de novo* transcription initiation. Ansamycin binding in the RIF-binding pocket inhibits transcription by clashing with the 5′ end of a nascent RNA. Modeling shows that, in the *T. thermophilus* RNAP-RIF complex, the triphosphate moiety of the initiating nucleoside triphosphate (NTP) guided by hydrogen bonds with side chains of two essential residues, βQ567 and βH999 (Basu et al., 2014), moderately clashes with the C3 side chain of RIF (Figure 2E, right). This clash does not strongly affect the formation of the first phosphodiester bond, likely because of flexibility of the C3 side chain. Even in the presence of RIF, there is an empty space (triphosphate retreat zone) that allows for accommodation of the 5′ triphosphate group followed by an extension of the nascent RNA to 3-mer (McClure and Cech, 1978) before a severe clash with the +1 NTP inhibits further primer extension (Figure 2E, right). In contrast, the positional shift of KglA and the orientation of the negatively charged C20 2,2-dimethyl succinic acid side chain not only do not leave space for accommodation of the 5′ triphosphate group but also interfere with the correct placement of the initiating NTPs (Figure 2E, left), which explains the strong inhibition of the initial dinucleotide synthesis (Figure 1D). The electrostatic repulsion by the C20 2,2-dimethyl succinic acid side chain of KglA can also explain the inhibition of monophosphorylated pApUpC synthesis (which is allowed by RIF; Figure 1E).

A comparative analysis of the structures of the *E. coli* βS531L RNAP σ⁷⁰ holoenzyme in apo form and in complex with RIF and KglA reveals the mechanism of KglA's efficiency against many RIF-resistant forms of mutant RNAPs (Figure 2F). The amino acid substitution βS531L is the most clinically important RIF-resistant mutation in bacterial RNAP because of its low structural and functional effects on the enzyme in the absence of RIF. As shown in a recent study (Molodtsov et al., 2017), RIF binding to the mutant RNAP results in a steric clash of the naphthalene core with the side chain of β531L, which triggers disordering of a constituent part of the RIF-binding pocket, the fork loop2 (Figure 2F, left versus right). This partial disordering of the RIF-binding site efficiently prevents RIF binding. The naphthalene core of KglA is almost identical to RIF; however, it is rotated in the binding site compared with RIF (Figure 2D). This positional shift allows KglA to maintain a distance to β531L, avoiding a severe clash with the residue and minimizing structural rearrangements of the fork loop2 and the binding pocket (Figure 2F, center). This fine-tuning of the core binding mode and the increased interaction surface provided by the C27 sugar side chain enable high affinity of KglA in a broad context of RIF resistance.

Kanglemycin A Has Antimicrobial Activity against MDR-*M. tuberculosis* and Other Gram-Positive Pathogens

The above results suggested that KglA may be effective against RIF-resistant bacteria, in particular against clinically
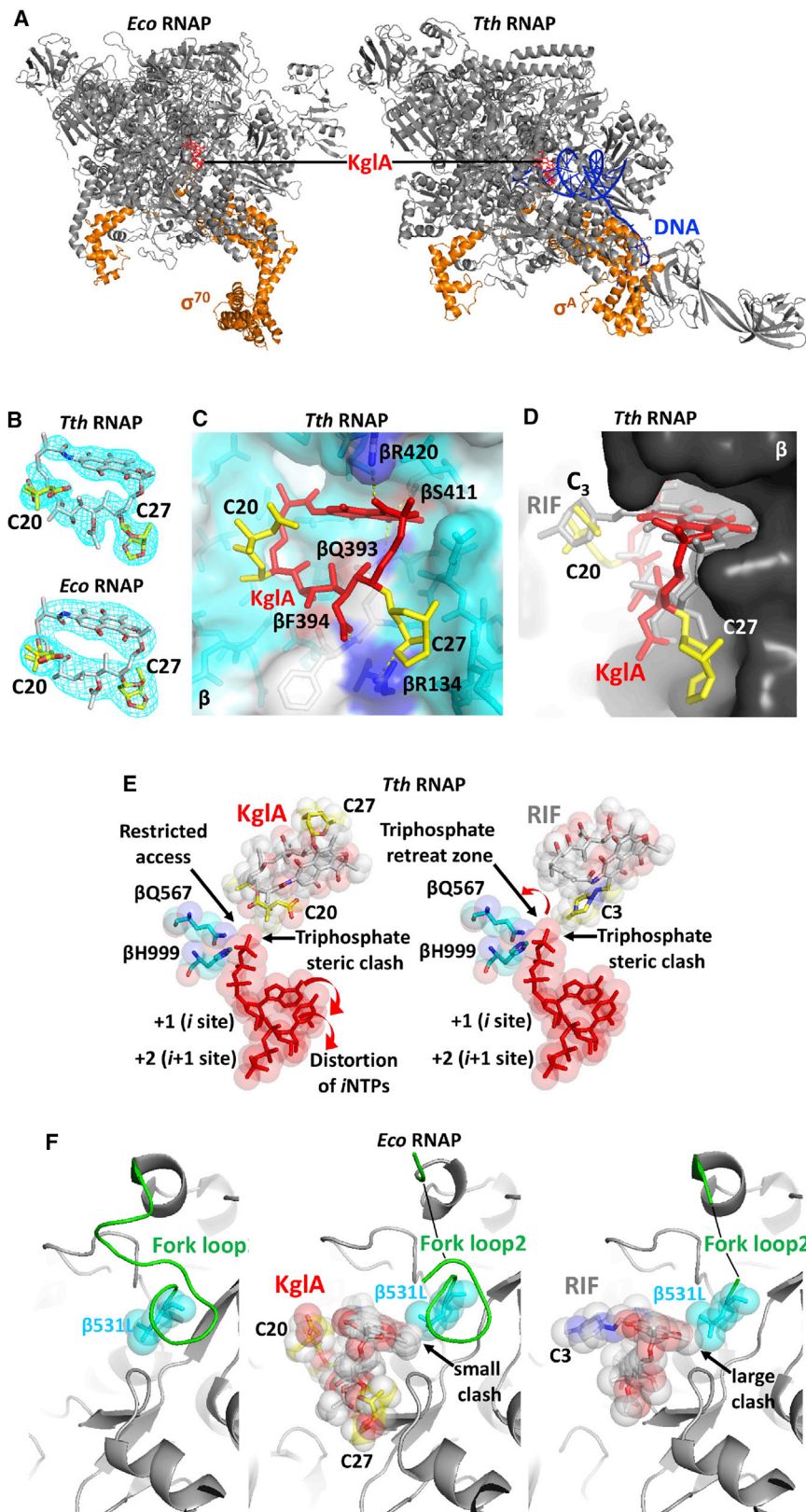
Figure 2. KglA Binding to Free and Promoter-Bound RNAP Holoenzyme

(A) Overall views of *E. coli* (left) and *T. thermophilus* (right) RNAPs with KglA bound in the RIF-binding pocket. RNAPs (gray core and orange σ) and DNA (blue) are shown as ribbon models, and KglA (red) is shown as a stick model.

(B) Electron density maps of KglA in complexes with *T. thermophilus* (top) and *E. coli* (bottom) RNAPs. Electron densities are shown as a light blue mesh, and KglA molecules are shown as stick models colored by element. The *ansa* bridge side chains of KglA extending from C20 and C27 are colored in yellow.

(C) A close-up view of the RIF-binding pocket of the *T. thermophilus* RNAP containing KglA (in red, with the side chains in yellow). RNAP is shown as a transparent surface model (light blue), KglA is shown as a stick model with the *ansa* bridge side chains labeled, and the β subunit residues forming the RIF-binding pocket are shown as stick models. The hydrogen bonds between KglA and β amino acid residues (colored by element) are depicted by yellow dotted lines; the βR134 involved in polar interaction with the C20 sugar of KglA is shown in blue.

(D) A side view of the RIF-binding pocket shown in (C). KglA is overlaid on RIF (gray); the side chains of the two molecules are labeled. KglA maintains a larger distance to the wall in the RIF-binding pocket than RIF.

(E) Modeling of the initiating nucleotides in the active site of the *T. thermophilus* RNAP (from PDB: 4Q4Z) in the presence of KglA (left) and RIF (right). The ribonucleotides (red), the βQ567 and βH999 residues coordinating the 5′ end triphosphate (blue), and KglA and RIF (gray) are shown as stick and sphere models. The side chains of the inhibitors and the positions of the initiating NTPs are indicated. Red arrows indicate the translocation directions for the corresponding substrates.

(F) Structural rearrangements in the RIF-binding pocket of *E. coli* βS531L RNAP triggered by KglA and RIF binding. RNAP is shown as a ribbon model in gray, the structured regions of the fork loop2 are shown in green, and the β531L residue (blue), KglA (colored by element with yellow side chains), and RIF (colored by element) are shown as stick and sphere models. The side chains of KglA and RIF are indicated. Arrows mark the clash points between the naphthalene cores of the corresponding compounds with the β531L side chain.
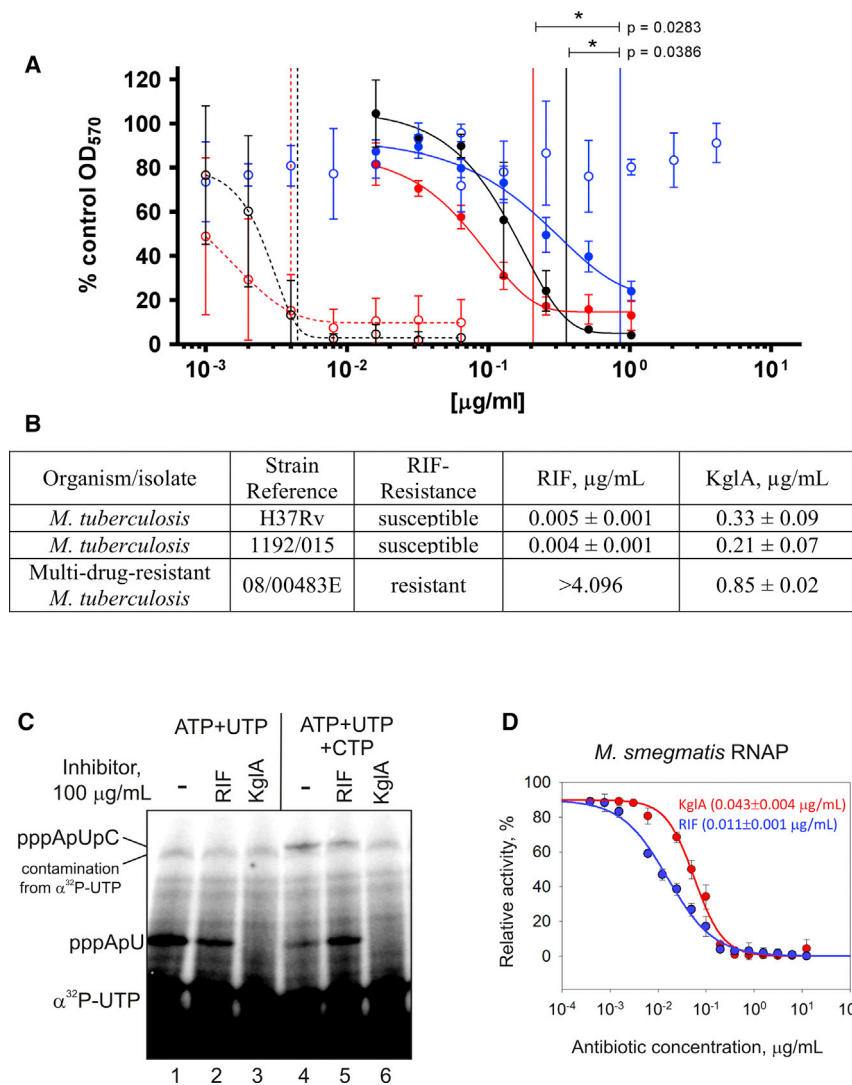
See also Figure S2.

Figure 3. KglA Inhibits Mycobacterial RNAP and Retains Antimicrobial Activity against MDR-*M. tuberculosis*

(A) Dose-dependent growth inhibition of the RIF-susceptible *M. tuberculosis* strains H36Rv (black) and 1192/015 (red) and RIF-resistant *M. tuberculosis* 08/00483E (blue) by KglA (solid line, solid symbols) and RIF (dashed line, open symbols). Data presented are the mean of four independent experiments ± SD and analyzed using a Student's t test.

(B) MIC values ± SD, as determined using the modified Gompertz function for *M. tuberculosis* strains H37Rv, 1192/015, and 08/00483E, which were exposed to RIF or KglA.

(C) Mode of action of KglA and RIF against *M. smegmatis* RNAP. The experiment was performed exactly as in Figure 1D. Note that the high radioactive background compared with Figure 1D is due to much lower activity of *M. smegmatis* RNAP.

(D) Inhibition of *M. smegmatis* RNAP by RIF and KglA.

Error bars are ± SD. Shown in brackets are the IC_{50} values ± SE.

B

Organism/isolate	Strain Reference	RIF-Resistance	RIF, µg/mL	KglA, µg/mL
M. tuberculosis	H37Rv	susceptible	0.005 ± 0.001	0.33 ± 0.09
M. tuberculosis	1192/015	susceptible	0.004 ± 0.001	0.21 ± 0.07
Multi-drug-resistant *M. tuberculosis*	08/00483E	resistant	>4.096	0.85 ± 0.02

problematic MDR-*M. tuberculosis* strains. Thus, we tested KglA against a clinical MDR-*M. tuberculosis* isolate (Beijing 08/00483E) that is fully resistant to RIF (Jamieson et al., 2014; Zhang et al., 2014b) and the other first-line antibiotics (isoniazid, ethambutol, and pyrazinamide). Beijing 08/00483E carries the most frequent RNAP amino acid change found in RIF-resistant *M. tuberculosis* (βS450L, *M. tuberculosis* numbering; βS531L, *E. coli* numbering; Figures S2C and S2D). As positive controls, we used the RIF-susceptible reference strain of *M. tuberculosis* H37Rv and a RIF-susceptible clinical isolate, Beijing 1192/015. The clinical strain Beijing 08/00483E was resistant to RIF at 1,024 times the minimum inhibitory concentration (MIC) for RIF-sensitive strains (Figures 3A and 3B). In contrast, all three strains displayed a dose-dependent response to KglA exposure (Figure 3A), demonstrating its antimicrobial activity against MDR-*M. tuberculosis*. KglA was statistically significantly more active against RIF-sensitive Beijing 1192/015 than RIF-resistant Beijing 08/00483E (Figures 3A and 3B).

As seen in Figures 3A and 3B, RIF was more active against RIF-susceptible *M. tuberculosis* cells than KglA. This apparently contradicted our *in vitro* results of very similar inhibition of *E. coli* wild-type RNAP by both inhibitors. It is possible that the mode of inhibition of *M. tuberculosis* RNAP by KglA is different from that of *E. coli* RNAP. Therefore, we analyzed inhibition of transcription by *Mycobacterium smegmatis* RNAP, which is commonly used as an experimental model for *M. tuberculosis* RNAP. Both RNAPs have an identical amino acid composition of the RIF-binding pocket (Figure S2C). We found that RIF and KglA inhibited RNA synthesis by *M. smegmatis* RNAP and *E. coli* RNAP in a very similar way (compare Figure 1D with Figure 3C); i.e., KglA fully blocked synthesis of the first dinucleotide (pppApU), whereas RIF partly allowed synthesis even of the trinucleotide (pppApUpC). The IC_{50} of KglA was nearly the same as that of RIF. Therefore, the affinity of RNAP binding cannot account for the observed difference in the activities of RIF and KglA against RIF-sensitive *M. tuberculosis* cells. The likely explanation of differences in activities of KglA and RIF against RIF-sensitive *M. tuberculosis* is the decreased ability of KglA to pass through the cell envelope.

We further tested KglA against a range of other species, including a number of clinically relevant pathogens. These included 8 Gram-positive bacteria, 10 Gram-negative bacteria, and 2 eukaryotes (Table 2). Of 10 Gram-negative pathogens, KglA was active against only *Providencia rettgeri*. No activity was observed toward the two strains of eukaryotic microorganisms (yeast): *Candida albicans* and *Candida glabrata*. Among the

Table 2. MICs of KglA against Bacterial and Eukaryotic Pathogens

	Organism/Isolate	Strain Reference	KglA (μg/mL)	RIF (μg/mL)
Gram-Negative	*Acinetobacter baumannii*	ATCC 19606	>128	–
	Burkholderia cepacia	ATCC 25416	>128	–
	Enterobacter cloacae	NCTC 11936	>128	–
	Escherichia coli	NCTC 10418	>128	16[a]
	Klebsiella pneumoniae	NCTC 9528	>128	–
	Providencia rettgeri	NCTC 7475	64	–
	Pseudomonas aeruginosa	NCTC 10662	>128	–
	Salmonella enterica Typhimurium	NCTC 74	>128	–
	Serratia marcescens	NCTC 10211	>128	–
	Yersinia enterocolitica	NCTC 11176	>128	–
Gram-Positive	*Bacillus subtilis*	NCTC 9372	1	–
	Enterococcus faecalis	NCTC 775	64	–
	Enterococcus faecium	NCTC 7171	128	–
	Listeria monocytogenes	NCTC 11994	8	–
	Staphylococcus epidermidis	NCTC 11047	1	–
	Staphylococcus aureus	NCTC 6571	0.25	0.004[a]
	Staphylococcus aureus (MRSA)	NCTC 11939	1	–
	Streptococcus pyogenes	NCTC 8306	0.031	–
Yeast	*Candida albicans*	ATCC 90028	>128	–
	Candida glabrata	NCPF 9725	>128	–
S. aureus	Bel	97597	2	2
	Bel	97598	64	>128
	Fin	37481	0.5	≤0.008
	Fin	54511	32	>128
	Fin	54518	128	>128
	Fra	462	0.5	≤0.008
	Fra	920	1	≤0.008
	Fra	95035	1	0.016
	Ger	131/98 (Sger 11d2)	0.5	0.016
	Ger	1966/97 (Han 111c)	0.5	≤0.008
	Ger	2594-1/97 (Sger 11a)	1	0.016
	Ger	2594-2/97 (Sger 11b)	0.25	≤0.008
	EMRSA 15	1729/98	0.5	≤0.008
	EMRSA 15	1758/98	0.5	≤0.008
	EMRSA 15	14956	0.5	≤0.008
	EMRSA 15	12484/98	0.5	≤0.008
	EMRSA 15	14185/98	0.5	≤0.008
	EMRSA 15	16822/98	0.5	≤0.008
	EMRSA 15	19972/98	0.5	≤0.008
	EMRSA 15	20460/98	0.5	0.016
	EMRSA 15	21268/98	0.5	≤0.008
	EMRSA 15	21698/98	0.5	≤0.008
	EMRSA 15	2501/98	0.5	≤0.008
	EMRSA 15	6323/98	0.5	≤0.008
	EMRSA 16	00036/95	1	0.016
	EMRSA 16	00998/95	1	≤0.008
	EMRSA 16	03732/95	1	0.016
	EMRSA 16	07121/95	1	≤0.008

(Continued on next page)

Table 2. *Continued*

	Organism/Isolate	Strain Reference	KglA (μg/mL)	RIF (μg/mL)
	EMRSA 16	07924/95	0.5	≤0.008
	EMRSA 16	18200/95	0.5	≤0.008
	EMRSA 16	18205/95	0.5	≤0.008
	EMRSA 16	21354/95	1	0.016
	EMRSA 16	23728/98	1	≤0.008
	EMRSA 16	23729/98	1	≤0.008
	EMRSA 16	32010/96	1	0.016
	EMRSA 16	34256/96	1	≤0.008
	MRSA	NCTC 11939	1	≤0.008
	Staphylococcus aureus	NCTC 6571	0.25	≤0.008

[a]Andrews (2001).

8 Gram-positive strains, KglA was highly active (MIC, ~1 μg/mL) against staphylococci and *Streptococcus pyogenes* but less active against enterococci (MIC, 64–128 μg/mL). The relatively high activity of KglA against staphylococci prompted evaluation of its activity against a large collection of methicillin-resistant *Staphylococcus aureus* (MRSA) and a comparison of its activity with RIF. *S. aureus* NCTC 6571 was re-tested as a control strain with a known MIC of RIF (EUCAST, 2018). Thirty-seven MRSA were tested in total, and 33 of these proved to be susceptible to RIF, as defined by a MIC of ≤ 0.06 μg/mL (EUCAST, 2018). KglA was substantially less active than RIF against RIF-susceptible MRSA, with MICs of KglA between 0.25 and 1 μg/mL. Conversely, for 3 of 4 RIF-resistant MRSA, MICs of KglA were 1–3 double dilutions lower than those of RIF, although still relatively high (32–128 μg/mL). In the light of our *in vitro* data (Figures 1C–1F and 3C), no activity against most of Gram-negative bacteria, and lower-than-RIF activity against some Gram-positive bacteria support the idea of a diminished ability of KglA to enter bacterial cells. This, however, requires further investigation coupled with further *in vivo* analyses to develop KglA as a future antibiotic.

DISCUSSION

Easily acquired RIF resistance is a major problem in the clinical usage of rifamycins. The principal finding of our study is that KglA is much more effective against RIF-resistant RNAPs and bacteria than its commonly used relative, RIF. The structural analysis suggests that this is explained by both additional interactions and the binding mode of KglA with RNAP unique to KglA. The sugar (β-O-3,4-O,O'-methylene digitoxose) and acid (2,2-dimethyl succinic acid) moieties at C27 and C20 of KglA, respectively, establish these additional contacts and influence the overall binding mode of KglA in the pocket (Figures 2C and 2D). Compared with RIF, KglA rotates to reposition slightly away (by 1.2 Å) from the wall of the binding pocket, which may decrease the effect of resistance mutations arising in RNAP on its affinity. Thus, the increased distance between the naphthalene core along with the increased binding surface provided by the *ansa*-bridge side chains likely represent the mechanisms that enable KglA to maintain its inhibitory activity against many

RIF-resistant bacterial RNAPs. As the result of additional interactions by the sugar moiety with the protein, only an unlikely event of two simultaneous mutations in the RIF-binding pocket can lead to KglA resistance.

KglA inhibits RNA synthesis at the stage of the first phosphodiester bond (2-mer RNA) formation, which is different from RIF, which inhibits formation of the second phosphodiester bond (3-mer RNA) (Figures 1D and 2E). Our biochemical and structural data suggest that this may happen because of the steric and/or electrostatic clash of the C20 2,2-dimethyl succinic acid side chain of KglA with γ and/or β phosphates of the +1 NTP that may disturb the conformation of initiating nucleotides and, thus, catalysis. We cannot directly compare these results with the previous study that found that some rifamycins may inhibit RNA synthesis one step earlier than RIF (Artsimovitch et al., 2005) because they used a 5′ non-phosphorylated dinucleotide to start transcription. We, however, did not observe inhibition of 5′ non-phosphorylated trinucleotide synthesis by KglA (Figure 1C), as observed for some of the rifamycins in that study (Artsimovitch et al., 2005), suggesting that inhibition of 5′ triphosphorylated dinucleotide synthesis by KglA takes place via a different mechanism.

KglA, compared with RIF, appears to show reduced penetration through the bacterial cell envelope, likely because of the presence of the polar carboxyl group at C20. For example, KglA has minimal activity against Gram-negative bacteria in comparison with RIF and displays higher MICs than RIF against most of the Gram-positive species tested. However, KglA is more effective than RIF against RIF-resistant Gram-positive bacteria. Notably, it is effective against MDR-*M. tuberculosis*. KglA inhibited the growth of MDR-*M. tuberculosis* (strain 08/00483E at a MIC of 0.854 μg/mL [850.3 nM]), which was completely resistant to RIF because of a βS450L substitution (βS531L in *E. coli* numbering). Finding new antibiotics for the treatment of MDR-TB is a challenge, and KglA demonstrates potential as a candidate for further development, particularly in light of the fact that the MIC of KglA is lower than the MIC values displayed for both isoniazid and pyrazinamide against drug-susceptible *M. tuberculosis*, and there is a wealth of information about drug toxicity and patient responses to RIF. These considerations are likely to accelerate the progression of KglA or its derivatives

to the clinic for the treatment of both drug-susceptible and drug-resistant TB.

A new mode of KglA binding to RNAP may enrich the strategy of structure-guided antibiotic design against RIF-resistant pathogens such as MDR-*M. tuberculosis*. RIF resistance caused by a point mutation of the β subunit of RNAP is associated with either loss of important contact between a target and a compound (in the case of βS531L) or steric exclusion of a compound from its binding site (in the case of βH526Y) (Molodtsov et al., 2017). In many cases, research efforts focusing on developing new antibiotics targeting the RIF-resistant bacterial RNAP are searching for new interaction surfaces away from the RIF-binding pocket (Lin et al., 2017; Maffioli et al., 2017). The enhanced affinity of KglA for certain RIF-resistant RNAPs along with the moderate changes in its mode of binding compared with RIF (Figure 2D) indicate that the RIF-binding pocket still possesses significant potential for the development of potent antibiotics against certain RIF-resistant pathogens. Targeting the RIF-binding pocket has some advantages compared with targeting a new site. For example, development of resistance to KglA is possible via additional mutations in the RIF-binding pocket (e.g., βR143A; Figure S2E) in addition to the first RIF-resistant mutation (e.g., βS531L); however, such mutations may compromise the transcriptional integrity and further diminish the fitness of the RNAP, rendering the resulting pathogens non-viable (Song et al., 2014). Another important advantage of developing new rifamycin derivatives is that this approach exploits the well-known rifamycin scaffold and may likely overcome some obstacles common in the development of new antibiotics, such as the problems of drug permeability through bacterial membranes, human toxicity, and specificity (Aristoff et al., 2010).

The modifications in the *ansa* bridge are highly unusual in bioactive rifamycins, with even minor semisynthetic modifications in an *ansa* bridge often leading to loss of RNAP inhibition (see Introduction). Our study reveals the significant potential of increasing the affinity of the rifamycins to RNAP via *ansa* bridge modifications, in particular by demonstrating that C27 substitution can allow access to a previously unexplored hydrophobic pocket adjacent to the RIF-binding pocket while maintaining the critical interactions between the rifamycin backbone and the RIF-binding pocket of RNAP. Furthermore, substitution at C20 with a flexible carboxylic acid residue has revealed the potential for new drug-initiating NTP interactions in the rifamycins. Altogether, KglA provides an example of an evolved solution to RIF resistance in which these unusual *ansa* bridge modifications lead to improved potency against RIF-resistant RNAPs and represents an important starting point for the development of new therapeutic agents.

STAR★METHODS

Detailed methods are provided in the online version of this paper and include the following:

- KEY RESOURCES TABLE
- CONTACT FOR REAGENT AND RESOURCE SHARING
- METHOD DETAILS
  - Disk diffusion assay
  - Isolation of KglA from Amycolatopsis sp. DEM30355
  - Small molecule X-ray crystallography including absolute configuration of KglA
  - NMR analysis of KglA
  - Purification of *E. coli* RNAP core enzyme and σ70, and **M. smegmatis RNAP holoenzyme** for transcription assays
  - *In vitro* transcription
  - Crystallization of RNAP – KglA complexes
  - Crystallographic data collection and X-ray crystal structure determinations
  - Determination of minimum inhibitory concentrations (MICs) for *M. tuberculosis*
  - Determination of minimum inhibitory concentrations for other bacteria
- DATA AND SOFTWARE AVAILABILITY

AUTHOR CONTRIBUTIONS

H.M., L.C., J.H., and Y.Y. performed biological experiments and analyzed the data. B.K., S.M.L., and N.E.E.A. purified KglA. V.M., Y.S., and K.S.M. performed crystallographic experiments and analyzed the structures. M.J.H., S.M.L., and C.W. performed the NMR analysis and structural assignment of KglA. W.C. performed small-molecule X-ray crystallography. C.W.M., R.E.J., and J.B. measured the MICs for the *M. tuberculosis* strains. J.D.P. and E.C.L.M. measured KglA MICs for other species. J.E., N.E.E.A., and N.Z. conducted the study. J.B., C.W.M., V.M., M.J.H., K.S.M., and N.Z. wrote the paper.

REFERENCES

Adams, P.D., Afonine, P.V., Bunkóczi, G., Chen, V.B., Davis, I.W., Echols, N., Headd, J.J., Hung, L.-W., Kapral, G.J., Grosse-Kunstleve, R.W., et al. (2010). PHENIX: a comprehensive Python-based system for macromolecular structure solution. Acta. Cryst. *D66*, 213–221.

Afonine, P.V., Mustyakimov, M., Grosse-Kunstleve, R.W., Moriarty, N.W., Langan, P., and Adams, P.D. (2010). Joint X-ray and neutron refinement with phenix.refine. Acta Crystallogr. D Biol. Crystallogr. *66*, 1153–1163.

Andrews, J.M. (2001). Determination of minimum inhibitory concentrations. J. Antimicrob. Chemother. *48* (*Suppl 1*), 5–16.

Aristoff, P.A., Garcia, G.A., Kirchhoff, P.D., and Showalter, H.D. (2010). Rifamycins–obstacles and opportunities. Tuberculosis (Edinb.) *90*, 94–118.

Artsimovitch, I., Vassylyeva, M.N., Svetlov, D., Svetlov, V., Perederina, A., Igarashi, N., Matsugaki, N., Wakatsuki, S., Tahirov, T.H., and Vassylyev, D.G. (2005). Allosteric modulation of the RNA polymerase catalytic reaction is an essential component of transcription control by rifamycins. Cell *122*, 351–363.

Bacchi, A., Pelizzi, G., Nebuloni, M., and Ferrari, P. (1998). Comprehensive study on structure-activity relationships of rifamycins: discussion of molecular and crystal structure and spectroscopic and thermochemical properties of rifamycin O. J. Med. Chem. *41*, 2319–2332.

Bacchi, A., Carcelli, M., and Pelizzi, G. (2008). Sampling rifamycin conformational variety by cruising through crystal forms: implications for polymorph screening and for biological models. New J. Chem. *32*, 1725–1735.

Bae, B., Nayak, D., Ray, A., Mustaev, A., Landick, R., and Darst, S.A. (2015). CBR antimicrobials inhibit RNA polymerase via at least two bridge-helix cap-mediated effects on nucleotide addition. Proc. Natl. Acad. Sci. USA *112*, E4178–E4187.

Basu, R.S., Warner, B.A., Molodtsov, V., Pupov, D., Esyunina, D., Fernández-Tornero, C., Kulbachinskiy, A., and Murakami, K.S. (2014). Structural basis of transcription initiation by bacterial RNA polymerase holoenzyme. J. Biol. Chem. *289*, 24549–24559.

Bauer, A.W., Kirby, W.M., Sherris, J.C., and Turck, M. (1966). Antibiotic susceptibility testing by a standardized single disk method. Am. J. Clin. Pathol. *45*, 493–496.

Campbell, E.A., Korzheva, N., Mustaev, A., Murakami, K., Nair, S., Goldfarb, A., and Darst, S.A. (2001). Structural mechanism for rifampicin inhibition of bacterial rna polymerase. Cell *104*, 901–912.

Campbell, E.A., Pavlova, O., Zenkin, N., Leon, F., Irschik, H., Jansen, R., Severinov, K., and Darst, S.A. (2005). Structural, functional, and genetic analysis of sorangicin inhibition of bacterial RNA polymerase. EMBO J. *24*, 674–682.

Degen, D., Feng, Y., Zhang, Y., Ebright, K.Y., Ebright, Y.W., Gigliotti, M., Vahedian-Movahed, H., Mandal, S., Talaue, M., Connell, N., et al. (2014). Transcription inhibition by the depsipeptide antibiotic salinamide A. eLife *3*, e02451.

Emsley, P., and Cowtan, K. (2004). Coot: model-building tools for molecular graphics. Acta Crystallogr. D Biol. Crystallogr. *60*, 2126–2132.

EUCAST (2018). European Committee on Antimicrobial Susceptibility Testing. http://www.eucast.org/clinical_breakpoints/.

Floss, H.G., and Yu, T.W. (2005). Rifamycin-mode of action, resistance, and biosynthesis. Chem. Rev. *105*, 621–632.

Gill, S.K., and Garcia, G.A. (2011). Rifamycin inhibition of WT and Rif-resistant Mycobacterium tuberculosis and Escherichia coli RNA polymerases in vitro. Tuberculosis (Edinb.) *91*, 361–369.

Gold, B., Roberts, J., Ling, Y., Lopez Quezada, L., Glasheen, J., Ballinger, E., Somersan-Karakaya, S., Warrier, T., and Nathan, C. (2016). Visualization of the Charcoal Agar Resazurin Assay for Semi-quantitative, Medium-throughput Enumeration of Mycobacteria. J. Vis. Exp. *118*, 54690.

Ho, M.X., Hudson, B.P., Das, K., Arnold, E., and Ebright, R.H. (2009). Structures of RNA polymerase-antibiotic complexes. Curr. Opin. Struct. Biol. *19*, 715–723.

James, B.W., Williams, A., and Marsh, P.D. (2000). The physiology and pathogenicity of Mycobacterium tuberculosis grown under controlled conditions in a defined medium. J. Appl. Microbiol. *88*, 669–677.

Jamieson, F.B., Guthrie, J.L., Neemuchwala, A., Lastovetska, O., Melano, R.G., and Mehaffy, C. (2014). Profiling of rpoB mutations and MICs for rifampin and rifabutin in Mycobacterium tuberculosis. J. Clin. Microbiol. *52*, 2157–2162.

Julius, C., and Yuzenkova, Y. (2017). Bacterial RNA polymerase caps RNA with various cofactors and cell wall precursors. Nucleic Acids Res. *45*, 8282–8290.

Kashlev, M., Nudler, E., Severinov, K., Borukhov, S., Komissarova, N., and Goldfarb, A. (1996). Histidine-tagged RNA polymerase of Escherichia coli and transcription in solid phase. Methods Enzymol. *274*, 326–334.

Kepplinger, B., Morton-Laing, S., Seistrup, K.H., Marrs, E.C.L., Hopkins, A.P., Perry, J.D., Strahl, H., Hall, M.J., Errington, J., and Allenby, N.E.E. (2018). Mode of Action and Heterologous Expression of the Natural Product Antibiotic Vancoresmycin. ACS Chem. Biol. *13*, 207–214.

Lambert, R.J., and Pearson, J. (2000). Susceptibility testing: accurate and reproducible minimum inhibitory concentration (MIC) and non-inhibitory concentration (NIC) values. J. Appl. Microbiol. *88*, 784–790.

Lancini, G., and Zanichelli, W. (1977). Structure-activity relationship in rifamycins, Structure-activity relationships among the semisynthetic antibiotics edn (New York: Academic Press).

Lin, W., Mandal, S., Degen, D., Liu, Y., Ebright, Y.W., Li, S., Feng, Y., Zhang, Y., Mandal, S., Jiang, Y., et al. (2017). Structural Basis of Mycobacterium tuberculosis Transcription and Transcription Inhibition. Mol. Cell *66*, 169–179.e8.

Maffioli, S.I., Zhang, Y., Degen, D., Carzaniga, T., Del Gatto, G., Serina, S., Monciardini, P., Mazzetti, C., Guglierame, P., Candiani, G., et al. (2017). Antibacterial Nucleoside-Analog Inhibitor of Bacterial RNA Polymerase. Cell *169*, 1240–1248.e23.

McClure, W.R., and Cech, C.L. (1978). On the mechanism of rifampicin inhibition of RNA synthesis. J. Biol. Chem. *253*, 8949–8956.

Molodtsov, V., Fleming, P.R., Eyermann, C.J., Ferguson, A.D., Foulk, M.A., McKinney, D.C., Masse, C.E., Buurman, E.T., and Murakami, K.S. (2015). X-ray crystal structures of Escherichia coli RNA polymerase with switch region binding inhibitors enable rational design of squaramides with an improved fraction unbound to human plasma protein. J. Med. Chem. *58*, 3156–3171.

Molodtsov, V., Scharf, N.T., Stefan, M.A., Garcia, G.A., and Murakami, K.S. (2017). Structural basis for rifamycin resistance of bacterial RNA polymerase by the three most clinically important RpoB mutations found in Mycobacterium tuberculosis. Mol. Microbiol. *103*, 1034–1045.

Mukherjee, R., and Chatterji, D. (2008). Stationary phase induced alterations in mycobacterial RNA polymerase assembly: A cue to its phenotypic resistance towards rifampicin. Biochem. Biophys. Res. Commun. *369*, 899–904.

Mukhopadhyay, J., Das, K., Ismail, S., Koppstein, D., Jang, M., Hudson, B., Sarafianos, S., Tuske, S., Patel, J., Jansen, R., et al. (2008). The RNA polymerase "switch region" is a target for inhibitors. Cell *135*, 295–307.

Murakami, K.S. (2013). X-ray crystal structure of Escherichia coli RNA polymerase σ70 holoenzyme. J. Biol. Chem. *288*, 9126–9134.

Murakami, K.S., Shin, Y., Turnbough, C.L., Jr., and Molodtsov, V. (2017). X-ray crystal structure of a reiterative transcription complex reveals an atypical RNA extension pathway. Proc. Natl. Acad. Sci. USA *114*, 8211–8216.

Nateche, F., Martin, A., Baraka, S., Palomino, J.C., Khaled, S., and Portaels, F. (2006). Application of the resazurin microtitre assay for detection of multidrug resistance in Mycobacterium tuberculosis in Algiers. J. Med. Microbiol. *55*, 857–860.

Otwinowski, Z., and Minor, W. (1997). [20] Processing of X-ray diffraction data collected in oscillation mode. Methods Enzymol. *276*, 307–326.

Perlman, D. (1977). Structure-activity relationships among the semisynthetic antibiotics (New York: Academic Press).

Roghanian, M., Zenkin, N., and Yuzenkova, Y. (2015). Bacterial global regulators DksA/ppGpp increase fidelity of transcription. Nucleic Acids Res. *43*, 1529–1536.

Ryu, Y.J., Koh, W.J., and Daley, C.L. (2016). Diagnosis and Treatment of Nontuberculous Mycobacterial Lung Disease: Clinicians' Perspectives. Tuberc. Respir. Dis. (Seoul) *79*, 74–84.

Sandgren, A., Strong, M., Muthukrishnan, P., Weiner, B.K., Church, G.M., and Murray, M.B. (2009). Tuberculosis drug resistance mutation database. PLoS Med. *6*, e2.

Smith, A.J., and Savery, N.J. (2005). RNA polymerase mutants defective in the initiation of transcription-coupled DNA repair. Nucleic Acids Res. *33*, 755–764.

Song, T., Park, Y., Shamputa, I.C., Seo, S., Lee, S.Y., Jeon, H.S., Choi, H., Lee, M., Glynne, R.J., Barnes, S.W., et al. (2014). Fitness costs of rifampicin resistance in Mycobacterium tuberculosis are amplified under conditions of nutrient starvation and compensated by mutation in the β′ subunit of RNA polymerase. Mol. Microbiol. *91*, 1106–1119.

Tupin, A., Gualtieri, M., Leonetti, J.P., and Brodolin, K. (2010). The transcription inhibitor lipiarmycin blocks DNA fitting into the RNA polymerase catalytic site. EMBO J. *29*, 2527–2537.

Urban, A., Eckermann, S., Fast, B., Metzger, S., Gehling, M., Ziegelbauer, K., Rübsamen-Waigmann, H., and Freiberg, C. (2007a). Novel whole-cell antibiotic biosensors for compound discovery. Appl. Environ. Microbiol. *73*, 6436–6443.

Wang, N.J., Fu, Y., Yan, G.H., Bao, G.H., Xu, C.F., and He, C.H. (1988). Isolation and structure of a new ansamycin antibiotic kanglemycin A from a Nocardia. J. Antibiot. (Tokyo) *41*, 264–267.

World Health Organization (2017). Global tuberculosis report. CC BY-NC- SA 3.0 IGO.

Zenkin, N., Kulbachinskiy, A., Yuzenkova, Y., Mustaev, A., Bass, I., Severinov, K., and Brodolin, K. (2007). Region 1.2 of the RNA polymerase sigma subunit controls recognition of the -10 promoter element. EMBO J. *26*, 955–964.

Zhang, Y., Degen, D., Ho, M.X., Sineva, E., Ebright, K.Y., Ebright, Y.W., Mekler, V., Vahedian-Movahed, H., Feng, Y., Yin, R., et al. (2014a). GE23077 binds to the RNA polymerase 'i' and 'i+1' sites and prevents the binding of initiating nucleotides. eLife *3*, e02450.

Zhang, Z., Dai, F., Luo, F., Zhong, M., Huang, Z., Hou, T., and Xu, J. (2014b). Could high-concentration rifampicin kill rifampicin-resistant M. tuberculosis? Rifampicin MIC test in rifampicin-resistant isolates from patients with osteoarticular tuberculosis. J. Orthop. Surg. Res. *9*, 124.

STAR★METHODS

KEY RESOURCES TABLE

REAGENT or RESOURCE	SOURCE	IDENTIFIER
Bacterial and Virus Strains		
E. coli BL21(DE3)	Novagen	Cat# 69450
M. smegmatis mc^{2}155 (SM07)	Mukherjee and Chatterji, 2008	N/A
Mycobacterium tuberculosis H37Rv, Beijing 1192/015 and Beijing 08/00483E	PHE National Mycobacterial Reference Laboratory	N/A
E. coli T7 Express	New England BioLabs	Cat# C2566H
B. subtilis 168 *amyE::PhelD-lacZ cat*	Urban et al., 2007a	N/A
B. subtilis 168 *amyE::PhelD-lacZ cat rpoB$_{H482R}$*	This paper	N/A
Enterobacter cloacae	NCTC	NCTC 11936
Escherichia coli	NCTC	NCTC 10418
Klebsiella pneumoniae	NCTC	NCTC 9528
Providencia rettgeri	NCTC	NCTC 7475
Pseudomonas aeruginosa	NCTC	NCTC 10662
Salmonella typhimurium	NCTC	NCTC 74
Serratia marcescens	NCTC	NCTC 10211
Yersinia enterocolitica	NCTC	NCTC 11176
Bacillus subtilis	NCTC	NCTC 9372
Enterococcus faecalis	NCTC	NCTC 775
Enterococcus faecium	NCTC	NCTC 7171
Listeria monocytogenes	NCTC	NCTC 11994
Staphylococcus epidermidis	NCTC	NCTC 11047
Staphylococcus aureus	NCTC	NCTC 6571
Staphylococcus aureus (MRSA)	NCTC	NCTC 11939
Streptococcus pyogenes	NCTC	NCTC 8306
Candida glabrata	NCPF	NCPF 9725
Acinetobacter baumannii	ATCC	ATCC 19606
Burkholderia cepacia	ATCC	ATCC 25416
Candida albicans	ATCC	ATCC 90028
Clinical isolates of methicillin-resistant *Staphylococcus aureus* (MRSA) X 36.	Public Heath England, Colindale, UK	N/A
T. thermophilus HB8	ATCC	ATCC 27634
Chemicals, Peptides, and Recombinant Proteins		
Ni-NTA agarose	QIAGEN	Cat# 30230
HiTrap Q HP, 1 mL	GE Healthcare Life Sciences	Cat# 29051325
HiLoad 26/600 Superdex 200	GE Healthcare Life Sciences	Cat# 28989336
HiTrap Heparin HP, 5 mL	GE Healthcare Life Sciences	Cat# 17040601
HisTrap HP, 5 mL	GE Healthcare Life Sciences	Cat# 17524801
Bio-Rex 70 cation exchange resin	Bio-Rad	Cat# 1425842
Biotage® SNAP Ultra 100 g	Biotage	Cat# FSUL-0442-0100
[alpha-P32]Uridine 5′-triphosphate (UTP)	Hartmann Analytic	Cat# SRP-810
rNTP Set, 100 mM Solutions (ATP, CTP, GTP, UTP)	GE Healthcare	Cat# 27202501
QuikChange II kit (Stratagene)	Agilent	Cat# 200523
CpA	IBA Lifesciences	Cat# 5-0710-186
RIF	Sigma	Cat# R3501

(Continued on next page)

Continued

REAGENT or RESOURCE	SOURCE	IDENTIFIER
Resazurin sodium salt	Sigma	Cat# R7017
CMM MOD2	James et al., 2000	N/A
Middlebrook 7H9 medium	BD Difco	Cat# 271310
Phosphate buffered saline, pH 7.4	Severn Biotech	Cat# 20-74-10
IsoSensitest agar	Oxoid	Cat# CM0471
Amberlite XAD-16	Sigma	Cat# XAD16
Deposited Data		
KglA X-ray diffraction data	This paper	CCDC: 1827601 and 1827602
E. coli RNAP – KglA complex	This paper	PDB: 6CUX
T. thermophilus RNAP – KglA complex	This paper	PDB: 6CUU
E. coli RNAP	Murakami 2013	PDB: 4YG2
T. thermophilus RNAP – *pyrG* promoter complex	Murakami et al., 2017	PDB: 5VOI
Oligonucleotides		
See Table S2 for list of oligonucleotides		
Recombinant DNA		
pVS10(S531L)	Gill and Garcia, 2011	N/A
pGEMD	Murakami, 2013	N/A
pET21a-SigA	Basu et al., 2014	N/A
pETLrpoB	Smith and Savery, 2005	N/A
Software and Algorithms		
COOT	Emsley and Cowtan, 2004	https://www2.mrc-lmb.cam.ac.uk/personal/pemsley/coot/
HKL2000	Otwinowski and Minor, 1997	http://www.hkl-xray.com
PHENIX	Adams et al., 2010	https://www.phenix-online.org
Pymol	PyMOL	https://pymol.org/2/
Graphpad 7.00	Prism	https://www.graphpad.com/
SigmaPlot 11.0	Systat Software	https://systatsoftware.com/
Other		
VDX48 Plate with sealant	Hampton Research	Cat# HR3-275
12 mm x 0.22 mm Siliconized circle cover slides	Hampton Research	Cat# HR3-279
18 mm Mounted CryoLoop - 20 micron	Hampton Research	Cat# HR4-973
CrystalCap ALS with vial	Hampton Research	Cat# HR4-779
Vivaspin sample concentrator (MWCO 10 kDa)	GE Healthcare Life Sciences	Cat# 28-9323-60
Tecan Sunrise microplate absorbance reader	Tecan instruments	https://www.tecan.com/
Infinite M1000 multimode plate reader	Tecan instruments	https://www.tecan.com/
Isolaera ONE	Biotage	Cat# ISO-1SW
Jeol Lambda 500 MHz spectrometer	JEOL Ltd	N/A
Jeol ECS 400 MHz spectrometer	JEOL Ltd	N/A
Gemini X-ray Diffractometer/Atlas detector	Oxford Diffraction	N/A
Beam Station I19	National Synchrotron Facility Diamond Light Source	N/A

CONTACT FOR REAGENT AND RESOURCE SHARING

Further information and requests for resources and reagents should be directed to Lead Contact (n.zenkin@ncl.ac.uk).

METHOD DETAILS

Disk diffusion assay

Standard disc diffusion assay (Kirby-Bauer) was performed with the *B. subtilis* 168 *amyE::P_{helD}-lacZ cat* reporter strain or RIF-resistant *B. subtilis* 168 *rpoB_{H482R}* strain as described (Bauer et al., 1966). Briefly, disks were loaded with to 10 μg of each drug, air-dried and placed on nutrient agar plates with embedded lawn of bacteria and x-gal (100 μg/mL). Plates were incubated overnight at 37°C and scanned.

Isolation of KglA from Amycolatopsis sp. DEM30355

The fermentation of the *Amycolatiopsis* sp. DEM303555 was conducted as previously described. (Kepplinger et al., 2018). One kilogram of Amberlite XAD-16 resin was washed with deionized water and then applied to 50 L of filtered culture supernatant in batch absorption. The material was eluted with 32 L of 100% methanol and concentrated under reduced pressure (2.5 L). The concentrate was adjusted to pH 6.5 and extracted eight times with an equal amount of ethyl acetate. The organic extracts were combined and evaporated to dryness to yield 22.5 g of crude extract. A sample of the crude extract (3.91 g) was subjected to silica gel chromatography (eluent = 100% ethyl acetate, Biotage SNAP 100 g cartridge). KglA-containing fractions were combined and the solvent was removed under reduced pressure to give 1.24 g of a dark colored solid. This material was subjected to a second silica gel chromatography step (eluent = linear gradient from diethyl ether to ethyl acetate. Evaporation of the KglA containing fractions yielded 806.2 mg as an orange solid.

Small molecule X-ray crystallography including absolute configuration of KglA

Slow evaporation of a methanol solution of KglA gave crystals suitable for single-crystal X-ray analysis. The molecular structure of KglA was obtained to high precision using synchrotron radiation with a very small crystal of the methanol solvate at 120 K; all H atoms were located and freely refined. The short X-ray wavelength of 0.6889 Angstroms did not permit the determination of the absolute configuration, which was subsequently established unambiguously with CuKalpha radiation and a larger crystal, giving a molecular structure with otherwise slightly lower precision. CCDC 1827601 and 1827602 contain the supplementary crystallographic data for this paper, these data can be obtained free of charge from The Cambridge Crystallographic Data Centre (https://www.ccdc.cam.ac.uk/).

NMR analysis of KglA

All NMR spectra were recorded in $CDCl_3$ at 10°C. ^1H and $^{13}C\{^1H\}$ NMR spectra were recorded directly with a Jeol Lambda 500 MHz spectrometer (Figure S1), while ^1H COSY; 45, 90 and 135 DEPT; HMQC and HMBC were recorded with a Jeol ECS 400 MHz spectrometer (not shown). Proton and carbon assignment was performed *de novo* from both 1D and 2D NMR experiments and was in close agreement with the literature (Wang et al., 1988, Table S1).

Purification of *E. coli* RNAP core enzyme and σ^{70}, and *M. smegmatis* RNAP holoenzyme for transcription assays

RIF-resistant mutations were introduced in pETLRpoB plasmid (6xHis-tag on N terminus of β subunit of *E. coli* RNAP) (Smith and Savery, 2005) by site-directed mutagenesis using QuikChange II kit (Stratagene). Wild-type or mutant plasmids were transformed along with pACYCDuet-1_Ec_rpoZ (encoding for ω subunit) in T7 Express strain (New England Biolabs). Expression and purification of core RNAP was performed as described (Kashlev et al., 1996) (with heparin chromatography used instead of gel filtration as suggested). N-terminal 6xHis-tagged *E. coli* σ^{70} subunit was purified as described (Zenkin et al., 2007).

Cellular *M. smegmatis* RNAP holoenzyme with 6xHis-tag on C terminus of β' subunit was purified as *E. coli* RNAP above from *M. smegmatis* mc^{2}155 (SM07) (Mukherjee and Chatterji, 2008), with exception that cells were grown in MB-7H9 media supplemented with 0.05 Tween 80 and 2% glucose to late exponential phase.

In vitro transcription

One pmol of wild-type or mutant *E. coli* RNAP core and 3 pmols of σ^{70} (or one pmol of *M. smegmatis* holoenzyme) and 0.1 pmols of linear template containing T7A1 promoter (Julius and Yuzenkova, 2017; Roghanian et al., 2015) were mixed in 7 μL of transcription buffer (20 mM Tris HCl pH 7.9, 40 mM KCl, 10 mM $MgCl_2$). 1 μL of DMSO containing or not containing antibiotics (concentrations specified in Figures) was added to the reaction. Transcription was initiated by the addition of 2 μL of the mixture of nucleotides in transcription buffer, containing (final concentrations): 25 μM CpA or 0.5 mM ATP or 5 mM AMP with different combinations or all of 100 μM ATP, CTP and GTP and 10 μM α-[^{32}P]UTP (20 Ci/mmol) (Hartmann Analytic). Reactions were stopped after 10-min incubation at 37°C by the addition of formamide-containing loading buffer. Products were separated on 20% or 33% denaturing (8M urea) polyacrylamide gels, revealed by PhosphorImaging (GE Healthcare), and analyzed using ImageQuant software (GE Healthcare). Activities (a sum of run off and termination products) were normalized to the activity without antibiotic, which was taken as 100%. The average activity of at least three replicates for each concentration of antibiotic was plotted (with their standard deviations as error bars) against concentration and fitted in four parameter logistic equation by nonlinear regression using SigmaPlot. The averages and standard deviations of the three individual IC$_{50}$s are reported in Figure 1E.

Crystallization of RNAP – KglA complexes

The βS531L RIF-resistant mutant *E. coli* RNAP σ^{70} holoenzyme was prepared and crystallized as previously described (Molodtsov et al., 2017). The complex of the *T. thermophilus* RNAP σ^A holoenzyme bound to *pyrG* promoter was prepared and crystallized as previously described (Murakami et al., 2017). To prepare complexes of RNAPs with KglA, the RNAP crystals were soaked overnight at 22°C in the respective cryoprotection solutions supplemented with 1 mM KglA. After the soaking, crystals were frozen by plunging to liquid N$_2$.

Crystallographic data collection and X-ray crystal structure determinations

The X-ray diffraction datasets were collected at the Macromolecular Diffraction at the Cornell High Energy Synchrotron Source (MacCHESS) F1 beamline (Cornell University, Ithaca, NY) and the data were processed by HKL2000 (Otwinowski and Minor, 1997). Structures were determined by molecular replacement using the structures of the *E. coli* RNAP (Murakami, 2013) and the *T. thermophilus* RNAP – *pyrG* promoter complexes (Murakami et al., 2017) as corresponding initial search models. The structures were refined as the rigid body and the positional refinement with non-crystallographic symmetry and reference model structure restraints using the suite of programs Phenix (Afonine et al., 2010). The resulting electron density maps revealed clear maps corresponding to KglA that was not present in the initial search models, and the KglA model was fitted into the density maps using Coot (Emsley and Cowtan, 2004). The Table 1 contains data collection and refinement statistics for the structures of the determined RNAP – KglA complexes. The final coordinates and structure factors were deposited to the PDB with ID codes listed in Table 1.

Determination of minimum inhibitory concentrations (MICs) for *M. tuberculosis*
Bacterial strains and reagents

Mycobacterium tuberculosis strains: H37Rv, Beijing 1192/015 and Beijing 08/00483E (multi-drug resistant, MDR) were used in the modified resazurin microtiter assay (REMA) plate method. Beijing strains 1192/015 and 08/00483E were obtained from the PHE National Mycobacterial Reference Laboratory. Beijing 08/00483E contains a single nucleotide polymorphism (SNP) at position 761155 of C→T, which has resulted in an amino acid change, S450L (corresponding to S531L with *E. coli* numbering), within the RIF-binding pocket. Beijing 08/00483E is also resistant to isoniazid, ethambutol, and pyrazinamide, through mutations in known resistance genes. Other reagents used were: Middlebrook 7H9 medium (BD Difco), OADC supplemented with 0.5% glycerol (24388.295, VWR Chemicals) and 0.2% Tween 80 (P1754, Sigma), CAMR Mycobacterium Medium MOD2 (CMM MOD2) (James et al., 2000), RIF (PanReac AppliChem, cat no.A2220) and 0.02% resazurin solution (10 mg resazurin sodium salt (R7017, Sigma) in 50 mL phosphate buffered saline, pH 7.4 (Severn Biotech) containing 5% Tween 80) (Gold et al., 2016). All the antibiotics were dissolved in methanol (322415, Sigma) to a stock concentration of 10 mg/mL.

Preparation of bacterial inocula

Bacterial strains were grown in 50 mL of OADC-supplemented, Middlebrook 7H9 medium with 0.5% glycerol and 0.2% Tween 80 in vented Erlenmeyer flasks, shaken at 37°C for 5 days. Inocula for the REMA method were prepared to an OD$_{540}$ of 0.5, from Middlebrook 7H9 cultures by diluting cells in CMM MOD2 medium.

Modified resazurin microtiter assay (REMA) plate method

A modification of the REMA plate method previously described by (Nateche et al., 2006) was used. A 10 mg/mL stock solution of KglA was prepared in methanol (322415, Sigma). A two-fold serial dilution of the stock solution was performed in CMM MOD2 medium. 100 μl of each KglA concentration was added to six replicate wells in a 96-well untreated flat bottomed 96-well plate (734-1554, VWR). Three of the wells remained as "drug-only" wells and the other three wells were "test wells," which were used to test the activity of KglA. 10 μl of bacterial culture was added to the test wells to give a final OD$_{540}$ of 0.05. Three further wells contained 100 μl of growth medium and 10 μl of bacterial cells as "zero-drug" controls to confirm exponential growth of the bacteria in the absence of antibiotic. The drug-only controls allowed for confirmation that there was an absence of colorimetric interference from the candidate antibiotic. Bacterial cell samples were diluted to an optical density (OD$_{540}$) of 0.5 and 10 μl of the inoculum was added to each of the test wells and the zero drug controls. 10 μl of CMM MOD2 growth medium was added to the drug-only wells. The 96-well plates were incubated for 7 days at 37°C while shaking at 200 rpm. Drug activity was ascertained by adding 11 μl resazurin to every well of the 96 well-plate and incubating the plate at room temperature for 6 hours. The optical density (OD$_{570}$) was measured for each well. The OD$_{570}$ measurements were converted to a percentage of the zero-drug control so that data were expressed as a percentage of the growth without antibiotic.

Statistical analyses

The average OD$_{570}$ for each drug concentration was fitted to a sigmoidal curve using the modified Gompertz function ($y = A + Ce^{-e^{B(x - M)}}$) and the minimum inhibitory concentration (MIC) was identified from the point of inflexion of the lower asymptote (Lambert and Pearson, 2000). This was applied to the mean of the OD$_{570}$ of four biological repeats to produce a graphical representation for each condition. An unpaired, two tailed, Students t test was used to determine significance between biological repeats.

Determination of minimum inhibitory concentrations for other bacteria

MICs were determined using the agar dilution method specified by the British Society for Antimicrobial Chemotherapy against a collection of 56 isolates (Andrews, 2001). Briefly, KglA was initially dissolved in a minimal volume of dimethyl sulfoxide and diluted in water before incorporation into IsoSensitest agar (Oxoid) at a final concentration range of 128 – 0.031 μg/mL. A final inoculum

of 10 000 CFU/spot was used for inoculation of plates. Cultures were incubated for 22 hours at 37 ± 0.5°C. The MIC was recorded as the lowest concentration of KglA that achieved complete inhibition of visible growth. Inhibitor-free controls were also tested, including those containing equivalent solvent concentrations. All tests were performed at least twice on separate occasions to demonstrate reproducibility.

The collection included 16 isolates acquired from the National Collection of Type Cultures (NCTC; Colindale, UK), 3 isolates from the American Type Culture Collection (ATCC; Manassas, USA), and one from the National Collection of Pathogenic Fungi (NCPF; Colindale, UK). Also included were 36 strains of methicillin-resistant *Staphylococcus aureus* (MRSA) kindly supplied by Public Health England (Colindale, UK). These 36 strains were isolated from clinical samples in five European countries and included representatives of the major clones responsible for outbreaks of infection.

DATA AND SOFTWARE AVAILABILITY

The atomic coordinates and structure factors have been deposited in the Protein Data Bank, https://www.pdb.org (PDB ID codes 6CUX and 6CUU). CCDC 1827601 and 1827602 contain the supplementary crystallographic data for this paper, these data can be obtained free of charge from The Cambridge Crystallographic Data Centre (https://www.ccdc.cam.ac.uk/).

Supplemental Information

Mode of Action of Kanglemycin A, an Ansamycin

Natural Product that Is Active against

Rifampicin-Resistant *Mycobacterium tuberculosis*

Hamed Mosaei, Vadim Molodtsov, Bernhard Kepplinger, John Harbottle, Christopher William Moon, Rose Elizabeth Jeeves, Lucia Ceccaroni, Yeonoh Shin, Stephanie Morton-Laing, Emma Claire Louise Marrs, Corinne Wills, William Clegg, Yulia Yuzenkova, John David Perry, Joanna Bacon, Jeff Errington, Nicholas Edward Ellis Allenby, Michael John Hall, Katsuhiko S. Murakami, and Nikolay Zenkin

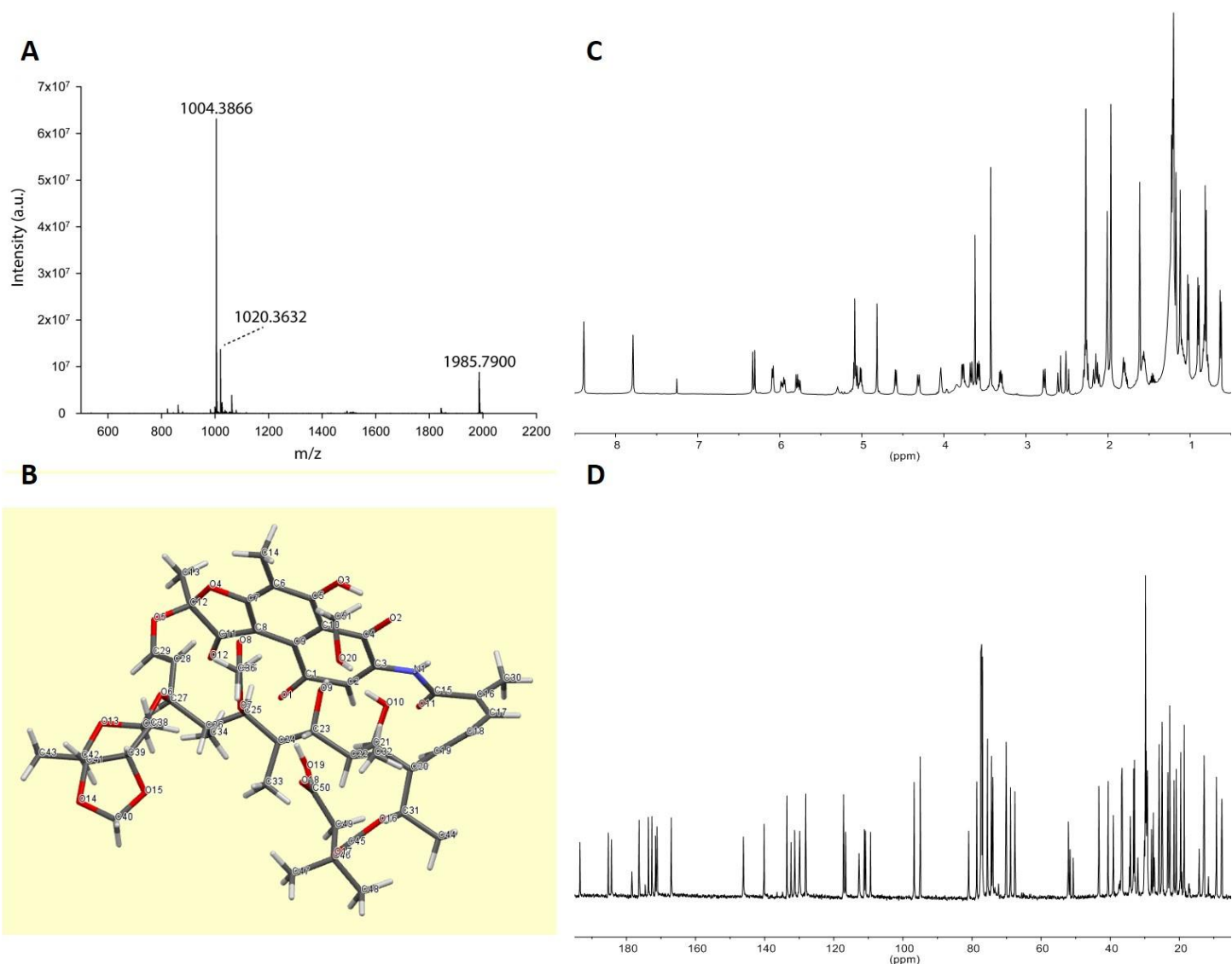**Figure S1.** *Related to Fig. 1B*. **A.** Mass spectrum of KglA showing peaks at 1004.3866, 1020.3632 and 1985.7900 Da, assigned as $[M+Na]^+$ $[M+K]^+$ and $[2M+Na]^+$ respectively. **B.** Crystallographically determined structure of KglA (from synchrotron data). Non-H atoms are labelled. **C.** 500 MHz ^{1}H NMR spectra of KglA in CDCl$_3$. **D.** 125 MHz ^{13}C{^{1}H} NMR spectra of KglA in CDCl$_3$.

Table S1. *Related to Fig. 1B.* Assignment of the ^{1}H and ^{13}C NMR data of KglA

Atom no.	δ_C	δ_H	Protons	Multiplicity	J (Hz)	^{1}H-^{1}H (COSY)	^{13}C-^{1}H (HMBC)
35	43.1	2.54	1	d	16.8	2.66 (**35**)	1.18 (**37**), 1.23 (**38**)
		2.66	1	d	16.8	2.54 (**35**)	
36	172.0	-	-	-	-	-	2.54 (**35**), 2.66 (**35**)
34	40.4	-	-	-	-	-	2.54 (**35**), 2.66 (**35**), 1.18 (**37**), 1.23 (**38**)
38	24.6	1.23	3	s	-	-	2.54 (**35**), 2.66 (**35**)
37	25.7	1.18	3	s	-	-	2.54 (**35**), 2.66 (**35**)
33	176.0	-	-	-	-	-	2.54 (**35**), 2.66 (**35**), 1.18 (**37**), 1.23 (**38**), 5.07 (**31**)
31	67.7	5.07	1	"q"	6.4	1.09 (**32**)	3.70 (**21**), 1.09 (**32**), 5.83 (**19**)
32	19.3	1.09	3	d	6.4	5.07 (**31**)	5.07 (**31**), 2.17 (**20**)
20	52.4	2.17	1	"t"	9.7	5.83 (**19**), 3.70 (**21**)	5.97 (**18**), 5.83 (**19**), 5.07 (**31**), 3.70 (**21**), 3.52 (OH), 1.87 – 1.81 (**22**)
19	133.6	5.83	1	dd	15.6, 9.7	5.97 (**18**), 2.17 (**20**)	6.17 (**17**), 5.97 (**18**), 5.07 (**31**), 3.70 (**21**), 2.17 (**20**), 2.06 (**30**)
18	127.9	5.97	1	dd	15.9, 6.2	6.17 (**17**), 5.83 (**19**)	5.83 (**19**), 2.17 (**20**), 2.06 (**30**)
17	129.6	6.17	1	"dt"	6.2, 1.3	5.97 (**18**), 2.06 (**30**)	5.97 (18), 5.83 (19), 2.06 (**30**)
16	132.5	-	-	-	-	-	5.97 (**18**), 5.83 (**19**), 2.06 (**30**)
30	20.5	2.06	3	s	-	6.17 (**17**)	6.17 (**17**)
15	171.0	-	-	-	-	-	8.35 (NH), 6.17 (**17**), 2.06 (**30**)
21	68.5	3.70	1	d	10.1	2.17 (**20**)	5.83 (**19**), 5.07 (**31**), 3.52 (OH), 2.86 (**23**), 2.17 (**20**), 1.87 – 1.81 (**22**), 0.95 (**39**)
22	33.5	1.87-1.81 (overlap **45**)	2[a]	m	-	0.95 (**39**)	2.86 (**23**), 2.17 (**20**), 0.95 (**39**)
39	12.4	0.95	3	d	7.0	1.87 – 1.81 (**22**)	3.70 (**21**), 2.86 (**23**), 1.87 – 1.81 (**22**)
23	78.5	2.86	1	d	10.3	1.60 (**24**)	4.39 (**25**), 3.70 (**21**), 1.87 – 1.81 (**22**), 1.60 (**24**), 0.95 (**39**), 0.70 (**40**)
24	36.6	1.60	1	m	-	2.86 (**23**), 0.70 (**40**), 4.39 (**25**)	2.86 (**23**), 0.70 (**40**), 1.87 – 1.81 (**22**)
40	8.9	0.70	3	d	6.7	1.60 (**24**)	4.39 (**25**), 2.86 (**23**), 1.60 (**24**)
25	73.7	4.39	1	d	9.9	2.13-2.08 (**26**), 1.60 (**24**)	3.86 (**27**), 2.86 (**23**), 2.06 (**30**), 0.70 (**40**), 0.39 (**43**)
41	173.6	-	-	-	-	-	4.39 (**25**), 2.03 (**42**)
42	21.3	2.03	3	s	-	-	-
26	36.7	2.13-2.08	1	m	-	0.39 (**43**), 4.39 (**25**), 3.86 (**27**)	5.14 (**28**), 4.39 (**25**), 3.86 (**27**), 0.39 (**43**)
43	12.9	0.39	3	d	7.2	2.13-2.08 (**26**)	4.39 (**25**), 3.86 (**27**), 2.13-2.08 (**26**)
27	80.9	3.86	1	dd	9.1, 3.0	5.14 (**28**), 2.13-2.08 (**26**)	6.37 (**29**), 4. 66 (**44**), 4.39 (**25**), 2.13-2.08 (**26**), 0.39 (**43**)
28	112.8	5.14 (overlap **47**)	2	dd	12.8, 9.1	3.86 (**27**), 6.37 (**29**)	6.37 (**29**), 3.86 (**27**),), 2.13-2.08 (**26**)
29	145.8	6.37	1	d	12.8	5.14 (**28**)	5.14 (**28**), 3.86 (**27**), 1.68 (**13**), 0.39 (**43**)
44	96.8	4.66	1	dd	8.9, 3.3	1.87 – 1.81 (**45**), 2.22 (**45**)	4.11 (**46**), 3.86 (**27**), 3.37 (**49**), 2.22 (**45**), 1.87 – 1.81 (**45**)
49	70.0	3.37	1	"dq"	9.0, 6.2	1.28 (**50**), 3.63 (**48**)	4.87 (**47**), 4.66 (**44**), 4.11 (**46**), 1.28 (**50**)
48	75.5	3.63	1	dd	9.0, 5.2	3.37 (**49**), 4.11 (**46**)	5.13 (**47**), 4.87 (**47**), 3.37 (**49**), 2.22 (**45**), 1.28 (**50**)
47	94.9	5.13 (overlap **28**)	2	"s"	-	-	3.63 (**48**)
		4.87	1	"s"	-	-	
46	74.3	4.11	1	"td"	4.8, 2.8	1.87 – 1.81 (**45**), 2.22 (**45**), 3.63 (**48**)	5.13 (**47**), 4.87 (**47**), 4.66 (**44**), 3.63 (**48**), 2.22 (**45**)
45	33.0	2.22	1	"dt"	14.5, 2.4	1.87 – 1.81 (**45**), 4.11 (**46**), 4.66 (**44**)	4.66 (**44**)
		1.87-1.81 (overlap **22**)	2[a]	m	-	2.22 (**45**), 4.11 (**46**), 4.66 (**44**)	
50	18.3	1.28	3	d	6.2	3.37 (**49**)	3.63 (**48**), 3.37 (**49**)
13	23.1	1.68	3	s	-	-	-
12	109.3	-	-	-	-	-	6.37 (**29**), 1.68 (**13**)
11	193.5	-	-	-	-	-	1.68 (**13**)
6	171.4	-	-	-	-	-	2.34 (**14**)
14	7.3	2.34	3	s	-	-	-
7	116.4	-	-	-	-	-	2.34 (**14**)
5	111.3	-	-	-	-	-	2.34 (**14**)
8	166.9	-	-	-	-	-	2.34 (**14**)
9	110.9	-	-	-	-	-	2.34 (**14**)
10	131.5	-	-	-	-	-	7.80 (**3**), 2.34 (**14**)
1/4	185.3	-	-	-	-	-	8.35 (NH), 7.80 (**3**)
1/4	184.3	-	-	-	-	-	8.34 (NH)
2	140.4	-	-	-	-	-	7.80 (**3**)
3	116.7	7.80	1	s	-	-	8.35 (NH)
NH	-	8.35	1	-	-	-	-
Ar-OH	-	12.60	1	-	-	-	-
OH (21)	-	3.52	1	-	-	-	-

[a]The integration of the signals in the 1.87 – 1.81 ppm region corresponded to 3 protons. 2 of these protons are assigned as C^{45}-H and C^{22}-H. It is possible that the remaining signal corresponds to an OH.
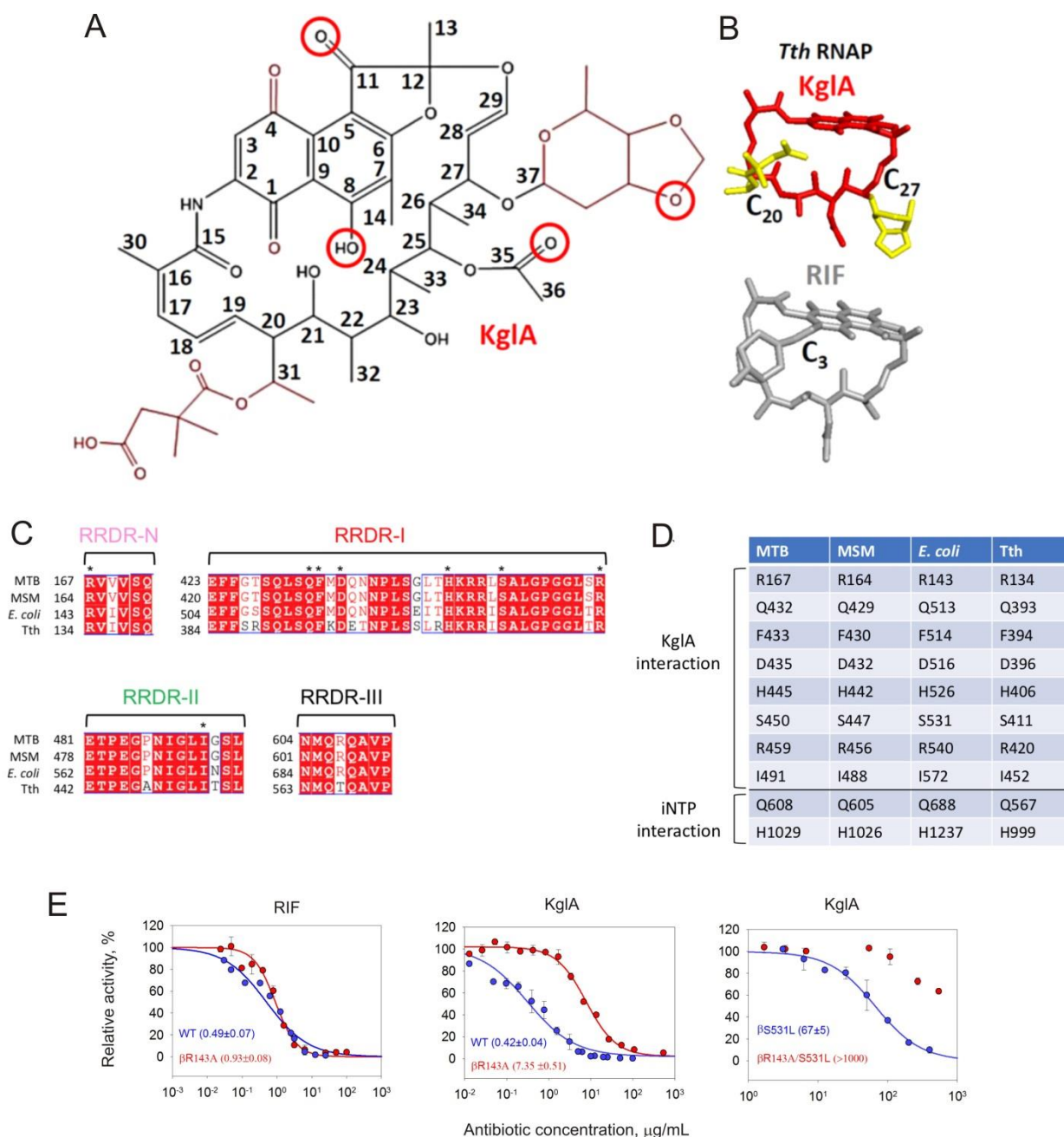
Figure S2. *Related to Fig. 2.* **A**. The chemical structure of Kanglemycin A (KglA). The four oxygen atoms forming hydrogen bonds with the RIF-binding pocket of RNAP are marked by red circles. **B.** Conformations of KglA and RIF in the RIF-binding pocket of *T. thermophilus* RNAP. KglA (red) and RIF (grey) are shown as stick models; the KglA's *ansa*-bridge C20 and C27 side chains are shown in yellow and labeled; the C3 side chain of RIF is labeled. **C.** Sequence alignment spanning the RIF resistance-determining regions (RRDRs) in the β subunit (RpoB) of RNAPs from *M. tuberculosis* H37RV (MTB), *M. smegmatis* (MSM), *E. coli* and *T. thermophilus* (Tth). Amino acid residues involved in the KglA interaction (Fig. 2) and also having mutations to generate the RIF-resistant RNAPs (Figs. 1 and 3) investigated in this study are indicated by asterisks.

D. Amino acid residues of the β subunit of RNAPs involved in the KglA and initiating NTP (iNTP) interactions. **E.** Involvement of KglA-specific interaction with βR143 in KglA activity. Error bars are ±SD. The brackets contain calculated IC50±SE. IC$_{50}$ of KglA for double mutant was beyond our measurement limit.

Table S2. Oligonucleotides used in the study.

Oligonucleotides		
D516V (GAC =>GTC) rpoB_D516V_d: GCT GTC TCA GTT TAT GGT CCA GAA CAA CCC GCT G rpoB_D516V_r: CAG CGG GTT GTT CTG GAC CAT AAA CTG AGA CAG C	This paper	N/A
S531L (TCC =>TTG) rpoB_S531_d: AAA CGT CGT ATC TTG GCA CTC GGC CC rpoB_S531_r: GGG CCG AGT GCC AAG ATA CGA CGT TT	This paper	N/A
H526P (CAC =>CCG) rpoB_H526Y_d: CTG AGA TTA CGC CGA AAC GTC GTA T rpoB_H526Y_r: ATA CGA CGT TTC GGC GTA ATC TCA G	This paper	N/A
H526Y (CAC =>TAC) rpoB_H526Y_d: CTG AGA TTA CGT ACA AAC GTC GTA T rpoB_H526Y_r: ATA CGA CGT TTG TAC GTA ATC TCA G	This paper	
I572F (ATC =>TTC) rpoB_I572_d: CAT CGG TCT GTT CAA CTC TCT GTC CG rpoB_I572_r: CGG ACA GAG AGT TGA ACA GAC CGA TG	This paper	N/A
Q513L (CAG =>CTG) rpoB_Q513L_d: CCA GCC AGC TGT CTC TGT TTA TGG ACC rpoB_Q513L_r: GGT CCA TAA ACA GAG ACA GCT GGC TGG	This paper	N/A
D516Y (GAC =>TAC) rpoB_D516Y_d: GCT GTC TCA GTT TAT GTA TCA GAA CAA CCC GCT G rpoB_D516Y_r: CAG CGG GTT GTT CTG ATA CAT AAA CTG AGA CAG C	This paper	N/A
H526R (CAC =>CGC) rpoB_H526R_d: CTG AGA TTA CGC GCA AAC GTC GTC G rpoB_H526R_r: CGA CGA CGT TTG CGC GTA ATC TCA G	This paper	N/A
D516V (GAC =>GTC) rpoB_D516V_d: GCT GTC TCA GTT TAT GGT CCA GAA CAA CCC GCT G rpoB_D516V_r: CAG CGG GTT GTT CTG GAC CAT AAA CTG AGA CAG C	This paper	N/A
S531L (TCC =>TTG) rpoB_S531_d: AAA CGT CGT ATC TTG GCA CTC GGC CC rpoB_S531_r: GGG CCG AGT GCC AAG ATA CGA CGT TT	This paper	N/A
H526P (CAC =>CCG) rpoB_H526Y_d: CTG AGA TTA CGC CGA AAC GTC GTA T rpoB_H526Y_r: ATA CGA CGT TTC GGC GTA ATC TCA G	This paper	N/A
H526Y (CAC =>TAC) rpoB_H526Y_d: CTG AGA TTA CGT ACA AAC GTC GTA T rpoB_H526Y_r: ATA CGA CGT TTG TAC GTA ATC TCA G	This paper	N/A
I572F (ATC =>TTC) rpoB_I572F_d: CAT CGG TCT GTT CAA CTC TCT GTC CG rpoB_I572F_r: CGG ACA GAG AGT TGA ACA GAC CGA TG	This paper	N/A
R143A (CGT=>GCT) rpoB_R143A_d: TGT TAT CAA CGG TAC TGA GGC TGT TAT CGT TTC CCA GCT G rpoB_R143A_r: CAG CTG GGA AAC GAT AAC AGC CTC AGT ACC GTT GAT AAC A	This paper	N/A
pyrG non-template: TAT AAT GGG AGC TGG CTC TGA TGC AGG _pyrG_ template: CCT GCA TCA GAG CCC AAA ATA C	Murakami et al., 2017	N/A